Antiviral Research 164 (2019) 162–175

Contents lists available at ScienceDirect

Antiviral Research

journal homepage: www.elsevier.com/locate/antiviral

Insight into the mechanism of action of EP-39, a bevirimat derivative that inhibits HIV-1 maturation

Aymeric Neyret[a], Bernard Gay[a], Anaïs Cransac[a], Laurence Briant[a], Pascale Coric[b], Serge Turcaud[c], Philippe Laugâa[b], Serge Bouaziz[b], Nathalie Chazal[a,*]

[a] Institut de Recherche en Infectiologie de Montpellier (IRIM), Université de Montpellier, CNRS, 1919 Route de Mende, 34293 Montpellier cedex 5, France
[b] CiTCoM, CNRS, UMR 8038, Université Paris Descartes, Sorbonne Paris Cité, 4 av. de l'Observatoire, Paris, France
[c] LCBPT, CNRS, UMR 8601, Université Paris Descartes, Faculté des Sciences Fondamentales et Biomédicales, 45 rue des Saints-Pères, 75006 Paris, France

ARTICLE INFO

Keywords:
HIV-1
Pr55Gag
Maturation
Maturation inhibitors
Assembly
NMR
Structure
Docking

ABSTRACT

Maturation of human immunodeficiency virus type 1 (HIV-1) particles is a key step for viral infectivity. This process can be blocked using maturation inhibitors (MIs) that affect the cleavage of the capsid-spacer peptide 1 (CA-SP1) junction. Here, we investigated the mechanisms underlying the activity of EP-39, a bevirimat (BVM) derivative with better hydrosolubility. To this aim, we selected *in vitro* EP-39- and BVM-resistant mutants. We found that EP-39-resistant viruses have four mutations within the CA domain (CA-A194T, CA-T200N, CA-V230I, and CA-V230A) and one in the first residue of SP1 (SP1-A1V). We also identified six mutations that confer BVM resistance (CA-A194T, CA-L231F, CA-L231M, SP1-A1V, SP1-S5N and SP1-V7A). To characterize the EP-39 and BVM-resistant mutants, we studied EP-39 effects on mutant virus replication and performed a biochemical analysis with both MIs. We observed common and distinct characteristics, suggesting that, although EP-39 and BVM share the same chemical skeleton, they could interact in a different way with the Gag polyprotein precursor (Pr55Gag). Using an *in silico* approach, we observed that EP-39 and BVM present different predicted positions on the hexameric crystal structure of the CA_{CTD}-SP1 Gag fragment. To clearly understand the relationship between assembly and maturation, we investigated the impact of all identified mutations on virus assembly by expressing Pr55Gag mutants. Finally, using NMR, we have shown that the interaction of EP-39 with a peptide carrying the SP1-A1V mutation (CA-SP1(A1V)-NC) is almost suppressed in comparison with the wild type peptide. These results suggest that EP-39 and BVM could interact differently with the Pr55Gag lattice and that the mutation of the first SP1 residue induces a loss of interaction between Pr55Gag and EP-39.

1. Introduction

Since the approval of zidovudine (AZT) in 1987, over 35 anti-retroviral drugs in six mechanistic classes have been approved for the HIV-1 treatment and shown to significantly increase patient survival. Indeed, antiretroviral therapy (ART) that uses various combinations of small molecule inhibitors has been highly effective in controlling the viral loads in infected individuals. However, issues associated with long-term toxicity, therapeutic compliance and the development of resistance remains a major cause of treatment failure. In order to address these problems, the discovery of antiretroviral drugs targeting new mechanisms of actions with improved safety profiles remains a high priority. Maturation inhibitors (MIs) represent a promising class of anti-HIV-1 compounds that specifically interfere with processing of the viral Gag polyprotein precursor (Pr55Gag) by a distinct mechanism of virus maturation inhibition from that exerted by HIV protease inhibitors (PIs). The small molecule 3-O(3′,3′-dimethylsuccinyl)-betulinic acid (DSB), also known as PA-457, MPC-4326 or bevirimat (BVM), was the first in class of this new family of anti-HIV-1 molecules (Fujioka et al., 1994; Kashiwada et al., 1996; Kanamoto et al., 2001; Li et al., 2003; Wainberg and Albert, 2010; Briant and Chazal, 2011; Sundquist and Kräusslich, 2012; Waheed and Freed, 2012; Freed, 2015; Wang et al., 2015). Although its development was stopped, BVM provided the clinical proof of concept that MIs might be an effective alternative for HIV-1 infection management. Recently, second-generation of BVM derivatives (Qian et al., 2010, 2012; Dang et al., 2013; Tang et al., 2014; Urano et al., 2015, 2018; Liu et al., 2016; Nowicka-Sans et al., 2016; Regueiro-Ren et al., 2016; Swidorski et al., 2016) have been developed to significantly increase the pan-genotypic coverage (Wang et al., 2015; Tang et al., 2017).

* Corresponding author. IRIM, UMR 9004-CNRS-Université Montpellier, 1919 Route de Mende, 34293 Montpellier cedex 5, France.
E-mail address: nathalie.chazal@irim.cnrs.fr (N. Chazal).

https://doi.org/10.1016/j.antiviral.2019.02.014
Received 27 November 2018; Received in revised form 19 February 2019; Accepted 22 February 2019
Available online 27 February 2019
0166-3542/

The formation of HIV-1 virions is driven by the viral Gag polyprotein precursor (Pr55Gag) that assembles into a lipid envelope-covered protein shell underneath the plasma membrane (Briant and Chazal, 2011; Briggs and Kräusslich, 2011; Freed, 2015; Ganser-Pornillos et al., 2012; Sundquist and Kräusslich, 2012). Pr55Gag contains four major structural domains: p17 matrix (MA), p24 capsid (CA), p7 nucleocapsid (NC) and p6 domain. A highly conserved sequence in the CA, named "Major Homology Region" (MHR), plays a critical role in HIV-1 assembly, maturation and infectivity. Two linker peptides, the spacer peptide 1 (SP1) and spacer peptide 2 (SP2), connect the CA and NC and the NC and p6 domains, respectively (Briant and Chazal, 2011; Freed, 2015; Konvalinka et al., 2015). After formation of immature virions and particle budding, Pr55Gag is cleaved in a sequential order by the viral protease (PR), allowing the release of mature MA, CA, NC and p6 and the elimination of SP1 and SP2. Completion of Pr55Gag processing is essential for virus maturation and infectivity (Briant and Chazal, 2011; Checkley et al., 2010; Freed, 2015; Ganser-Pornillos et al., 2012; Gross et al., 2000; Konvalinka et al., 2015; Kräusslich et al., 1995; Pettit et al., 1994; Wiegers et al., 1998). In this context, the dynamic helix-coil equilibrium in CA C-terminal domain-SP1 (CA_{CTD}-SP1) plays a key role in the mechanism of the final separation of CA from SP1, which is strictly required for the formation of the cone shaped capsid and of fully infectious virions (Datta et al., 2011; Accola et al., 1998; Pettit et al., 1994; Checkley et al., 2010; Wang et al., 2017). BVM interferes with the final PR-mediated Pr55Gag processing step by delaying SP1 release from CA C-terminus. In recent years, we structurally investigated the mechanisms underlying BVM activity by studying the interactions engaged in complexes formed by this MI with CA-SP1. To overcome the poor hydrosolubility of BVM that represents a barrier for NMR studies, we introduced a modification at the C-28 position to generate EP-39 (Fig. 1A) (Coric et al., 2013). The BVM-derivative EP-39, that does not block virus attachment or entry (data not shown), shows an improved hydrosolubility and inhibits HIV-1 maturation with a significantly higher selectivity index and stronger antiviral activity than BVM (Coric et al., 2013).

We previously described and conducted analysis on the EP-39 (Coric et al., 2013). Here, our goal was to investigate EP-39 specific inhibitory properties, compare the mechanisms of action of EP-39 and BVM. We find that EP-39 induces the production of a higher proportion of morphologically aberrant particles compared to BVM. Using a series of *in vitro* experiments, we identified a broad spectrum of replication-competent HIV-1 variants capable of conferring EP-39 or BVM resistance. Five and six single-amino-acid substitutions which independently confer EP-39 or BVM resistance were identified respectively. The characteristics of the EP-39 or BVM-resistant isolates were determined. The results of the *in silico* approach suggested that EP-39 and BVM could bind to the same binding pockets, with a different positioning on the hexameric crystal structure of CA_{CTD}-SP1. Finally, the NMR analysis showed that the interaction between EP-39 and the CA-SP1(A1V)-NC peptide, which harbors the SP1-A1V mutation, is almost abolished.

2. Materials and methods

2.1. EP-39 and BVM, cell culture and transfections

EP-39 and BVM were prepared as described previously (Coric et al., 2013) and used at the indicated concentrations. The H9-T cell line (single cell clone derived from a specific HUT 78 cell line, HT. HUT 78 is a human cutaneous T cell lymphoma, existing collection) was maintained in RPMI 1640 supplemented with 10% fetal calf serum (FCS, Cambrex). Human embryonic kidney (HEK) 293T cells were maintained in Dulbecco's modified Eagle's medium (DMEM) with 10% FCS (Life Technologies, Inc.) supplemented with 10% FCS (Cambrex), 100 units/mL penicillin, 100 µg/ml streptomycin. Plasmid DNAs were purified with the Qiagen Maxiprep Kit. HEK 293T cells were transfected using the JetPei transfection reagent (QBiogen).

2.2. Viral stock production

Viral stocks were generated as previously described (Brun et al., 2008). HEK 293T cells (Human embryonic kidney cells, existing collection) (3.5×10^5) were transfected with 3 µg of pNL4.3 DNA (AIDS Research and Reference Reagent Program, Division of AIDS, NIAID, NIH) or pNL4.3 mutants using Jet Pei (QBiogen). Two days after transfection, virus-containing supernatants were collected, filtered on 0.45 µM membranes, aliquoted and stored at −80 °C. All viral preparations were purified by centrifugation through 20% sucrose cushion. Pellets were resuspended in PBS, aliquoted and stored at −80 °C. Viral stocks were normalized according to p24 content using an anti-p24 Enzyme-linked Immunosorbent Assay (ELISA) (Ingen, France).

2.3. Selection for EP-39 and BVM resistance in vitro

EP-39 and BVM-resistant viral isolates were selected by serial passage of H9-T cells infected with wild type HIV-1 produced from HEK 293T cells transfected with WT pNL4-3. Infected H9-T cells were grown in the presence of 50 ng/ml BVM or 50 ng/ml EP-39 and split every 2 or 3 days, supernatants collected at each time point, and viral replication monitored with the anti-p24 ELISA (Ingen, France), as previously described (Giroud et al., 2013). Cell pellets and virus supernatants were harvested on the days of p24 peak. Infected cells were cultured as described above to confirm acquisition of BVM or EP-39 resistance. To identify mutations conferring BVM or EP-39 resistance, genomic DNA was extracted from cells on the day of p24 peak by using a whole-blood DNA purification kit (QIAGEN), and the entire Pr55Gag-PR-coding region was amplified by PCR using the forward and reverse primers NL516F (5′-TGC CCG TCT GTT GTG TGA CTC-3′) and NL2897R (5′-AAA ATA TGC ATC GCC CAC AT-3′). The 2.3-kb PCR product was purified using the QIAquick PCR Purification Kit (QIAGEN) and sequenced using the primers NL645F (5′-AAC AGG GAC TTG AAA GCG-3′), NL1155F (5′-AGG AAA CAA CAG CCA GGT-3′), NL1410F (5′-GGA AGC TGC AGA ATG GGA TA-3′), NL1754F (5′-TGG TCC AAA ATG CGA ACC-3′), and NL2135F (5′-TTC AGA GCA GAC CAG AGC CAA-3′(Adamson et al., 2006). Resistance-conferring mutations were introduced in the parental pNL4-3 sequence as described below.

2.4. Site-directed mutagenesis of pNL4-3

The 587-bp *Pst*I-*Apa*I fragment from pNL4-3 (nucleotides 1419 to 2006) was subcloned into pcDNA 3.1 (+) Zeo (Invitrogen). The CA-A194T, CA-T200N, CA-V230I, CA-V230A, SP1-S5N, SP1-V7A mutants were generated using the QuikChange Lightning Multi Site-Directed Mutagenesis Kit (Agilent technologies) and the following primers: for CA-194T: forward 5′CA GAA ACC TTG TTG GTC CAA AAT ACG AAC CCA GAT TGT AAG 3′ and reverse 5′CTT ACA ATC TGG GTT CGT ATT TTG GAC CAA CAA GGT TTC TG 3′; CA-T200N: forward 5′CCA GAT TGT AAG AAT ATT TTA AAA GCA TTG GGA CCA 3′ and reverse 5′TGG TCC CAA TGC TTT TAA AAT ATT CTT ACA ATC TGG 3′; CA-V230A: forward 5′C CAT AAG GCA AGA GCT TTG GCT GAA GCA ATG AGC 3′ and reverse 5′GCT CAT TGC TTC AGC CAA AGC TCT TGC CTT ATG G 3′; CA-V230I: forward 5′-C CAT AAG GCA AGA ATT TTG GCT GAA GCA ATG AGC 3′ and reverse 5′GCT CAT TGC TTC AGC CAA AAT TCT TGC CTT ATG G 3′; SP1-SN5: forward 5′GA GTT TTG GCT GAA GCA ATG AAC CAA GTA ACA AAT CCA GCT 3′ and reverse 5′ AGC TGG ATT TGT TAC TTG GTT CAT TGC TTC AGC CAA AAC TC 3′; and SP1-V7A: forward 5′ GCT GAA GCA ATG AGC CAA GCA ACA AAT CCA GCT ACC ATA 3′ and reverse 5′ TAT GGT AGC TGG ATT TGT TGC TTG GCT CAT TGC TTC AGC 3′. After confirmation of the mutations by sequencing, the *Sph*I-*Apa*I fragment was cloned back into WT pNL4-3 to create the molecular clones pNL4-3 CA-A194T, pNL4-3 CA-T200N, pNL4-3 CA-V230A, pNL4-3 CA-V230I, pNL4-3 SP1-S5N, pNL4-3 SP1-V7A that were confirmed by DNA sequencing.

The pNL4-3 CA-H226Y, pNL4-3 CA-L231F, pNL4-3 CA-L231M,

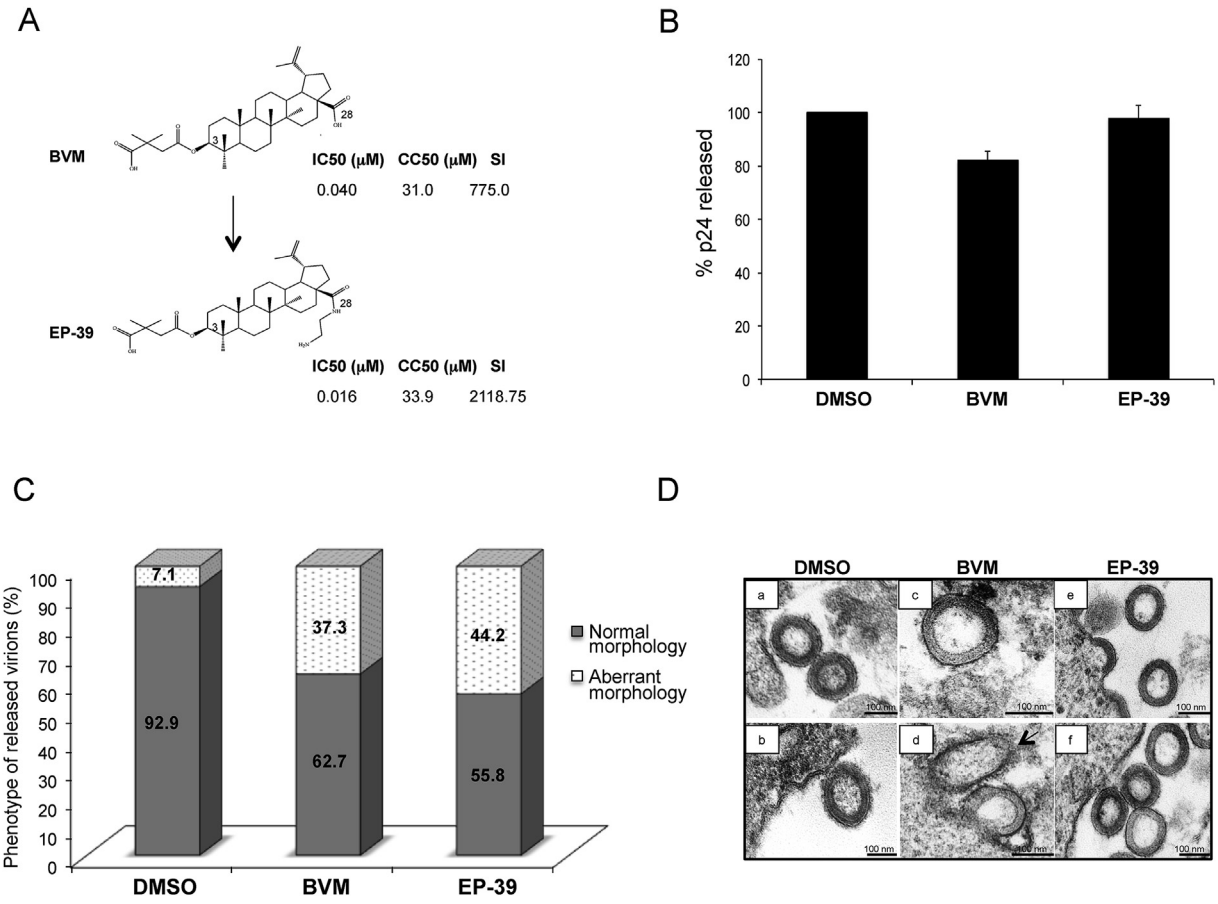

Fig. 1. HIV-1 particles release in the presence of EP-39 or BVM. (A) Structure of EP-39 and BVM. The C-3 and C-28 atoms are indicated in BVM backbone. The mean values (m) for the 50% inhibitory activity (IC_{50}) of infection were given as μM (m). The mean values (m) for cytotoxicity (CC_{50}) were given as μM (m). The selectivity index (SI) represented the CC_{50}/IC_{50} ratio (Coric et al., 2013). (B) HEK 293T cells were transfected with WT pNL4-3, few hours after transfection cells were split and cultured in the presence of 5 μg/ml of BVM or EP-39, or an equivalent volume of DMSO. Two days post-transfection, viral production in culture supernatants was monitored using an HIV-1 p24 ELISA kit (Ingen). Values are the mean ± SD of triplicate experiments. (C) Thin-section EM analysis: quantification of virions with normal or aberrant morphology released from the transfected HEK 293T cells described in (B) (n = 102–122). (D) Thin-section EM analysis of HEK 293T cells transfected with Pr55Gag expression plasmid. HEK 293T cells were transfected with the p55M1-10 plasmid to allow expression of full-length WT Pr55Gag and incubated with 5 μg/ml BVM (c,d) or EP-39 (e,f) or the equivalent concentration of DMSO (a,b). Two days post-transfection, cells were fixed and analyzed by thin-section EM, as previously reported (Brun et al., 2008) (Bar: ≈100 nm).

pNL4-3 SP1-A1V, pNL4-3 SP1-A3V and pNL4-3 SP1-A3T plasmids were kindly provided by E.O. Freed (Adamson et al., 2006).

2.5. Site-directed mutagenesis of Pr55Gag

All experiments were performed with derivatives of pCMV55M-10, the plasmid that directs Rev-independent expression of Pr55Gag in mammalian cells (Schneider et al., 1997). This plasmid was a kind gift by B. Felber (National Cancer Institute [NCI]). pCMV55M-10 was mutated to generate pCMV55M-10 CA-A194T, CA-H226Y, CA-T200N, CA-V230I, CA-V230A, CA-L231F, CA-L231M, SP1-A1V, SP1-A3V, SP1A3T, SP1-S5N, SP1-V7A using the QuikChange Lightning Multi Site-Directed Mutagenesis Kit (Agilent technologies) and the following primers: CA-A194T: forward 5′CAGAAACCTTGTTGGTCCAAAATACGAACCCAGAT TGTAAG 3′ and reverse 5′CTTACAATCTGGGTTCGTATTTTGGACCAA CAAGGTTTCTG 3’; CA-T200N: forward 5′ CCAGATTGTAAGAATATTT TAAAAGCATTGGGACCAGCGGC 3′ and reverse 5′ GCCGCTGG TCCCA ATGCTTTTAAAATATTCTTACAATCTGG 3’; CA-H226Y: forward 5′-GGGAGTAGGAGGACCCGGCTATAAGGCAAGAG 3′ and reverse 5′ CTCTTGCCTTATAGCCGGGTCCTCCTACTCCC 3’; CA-V230A: forward 5′CCATAAGGCAAGAGCTTTGGCTGAAGCAATGAGC 3′ and reverse 5′ GCTCATTGCTTCAGCCAAAGCTCTTGCCTTATGG 3’; CA-V230I: forward 5′ CCATAAGGCAAGAATTTTGGCTGAAGCAATGAGC 3′ and reverse 5′GCTCATTGCTTCAGCCAAAAT TCTTGCCTTATGG 3’; CA-L231F: forward 5′- TAAGGCAAGAGTTTTCGCTGAAGCAATGAGCC 3′ and reverse 5′ GGCTCATTGCTTCAGCGAAAACTCTTGCCTTA 3’; CA-L231M: forward 5′- TAAGGCAAGAGTTATGGCTGAAGCAATGAGCC 3′ and reverse 5′ GGCTCATTGCTTCAGCCATAAC TCTTGCCTTA 3’; SP1-A1V: forward 5′CAT AAG GCA AGA GTT TTG GTT GAA GCA ATG AGC CAA G 3′ and reverse 5′ C TTG GCT CAT TGC TTC AAC CAA AAC TCT TGC CTT ATG 3’; SP1-A3V: forward 5′C CAT AAG GCA AGA GTT TTG GCT GAA GTA ATG AGC CAA GTA AC 3′ and reverse 5′ GT TAC TTG GCT CAT TAC TTC AGC CAA AAC TCT TGC CTT ATG G 3’; SP1-A3T: forward 5′C CAT AAG GCA AGA GTT TTG GCT GAA ACA ATG AGC CAA GTA AC 3′ and reverse 5′ GT TAC TTG GCT CAT TGT TTC AGC CAA AAC TCT TGC CTT ATG G 3’; SP1-S5N: forward 5′GA GTT TTG GCT GAA GCA ATG AAC CAA GTA ACA AAT CCA GCT 3′ and reverse 5′ AGC TGG ATT TGT TAC TTG GTT CAT TGC TTC AGC CAA AAC TC 3’; and SP1-V7A forward 5′ GCT GAA GCA ATG AGC CAA GCA ACA AAT CCA GCT ACC ATA 3′ and reverse 5′ TAT GGT AGC TGG ATT TGT TGC TTG GCT CAT TGC TTC AGC 3’. Mutations were confirmed by DNA sequencing.

2.6. Immunoblotting analysis

All experiments were performed with HEK 293T cells. Culture

supernatant was harvested 48 h after transfection. After filtering through 0.45-µm-pore-size filters, virions or VLPs were then collected by centrifugation at 25,000 rpm in an SW28 rotor (Beckman) for 1 h through a cushion of 20% (wt/wt) sucrose. Cells, sucrose-purified virions and VLPs were solubilized in RIPA buffer and separated on 12.5% or 15% SDS-PAGE. Proteins were transferred to PVDF membrane (Millipore) and revealed using an anti-CA monoclonal antibody (Biogenesis) followed by incubation with a horseradish peroxidase-conjugated secondary antibody and enhanced chemiluminescence (Pierce Biotechnology Inc.).

2.7. Electron microscopy analysis

Virus-producing cells were processed for thin-layer electron microscopy as described elsewhere (Giroud et al., 2013). Briefly, cells were fixed *in situ* with 2.5% glutaraldehyde in phosphate buffer (pH 7.4) at 4 °C for 60 min. Cells were then post-fixed with 2% osmium tetroxide and then 0.5% tannic acid, dehydrated and embedded in Embed-812 (Electron Microscopy Sciences Inc.). Samples were examined with a Hitachi H.7100 transmission electron microscope (Plateau de microscopie Electronique COMET, INM, Montpellier RIO Imaging, Montpellier, France).

2.8. In silico docking

Docking was performed with the genetic algorithm-based GOLD (Genetic Optimization for Ligand Docking) Suite 5.2.1 from the Cambridge Crystallographic Data Center (Jones et al., 1995, 1997). The full hexameric crystal structure of the CA_{CTD}-SP1 Gag fragment (PBD ID 5I4T) (Wagner et al., 2016) was used as the target for docking. Incomplete or missing side chains were restored with the Dock Prep module of UCSF Chimera 1.8 using the Dunbrack rotamer library (Dunbrack, 2002). The whole hexamer surface was considered in the computations (i.e., neither specific site nor cavity was targeted). The hexamer was held rigid, whereas EP-39 and BVM were fully flexible. For each ligand, 100 poses were calculated and evaluated using the Chemscore score function. Otherwise, standard default parameter settings were used.

2.9. NMR analysis

The interaction between EP-39 and wild type CA-SP1-NC (48 aa; 211-231 CA, 1-14 SP1, 1-13 NC) or mutated CA-SP1(A1V)-NC was studied by NMR by performing 2D 1H-NOESY experiments (Jeener et al., 1979). All spectra were acquired at 293 K on a Bruker Avance 600 MHz spectrometer equipped with a 5 mm triple resonance probe and triple axis pulsed field gradients. NMR spectra were obtained using 250 µM of wild type or mutated peptide in the presence/absence of 550 µM EP-39 to attempt to observe an interaction at pH 3.8, in a H_2O/TFE (70/30) mixture to prevent aggregation and 1% DMSO-d_6. Chemical shifts were referenced to the H_2O resonance. NOESY spectra were acquired with 512 t1 and 2048 t2 complex points and 16 scans per increment. Spectral widths were set to 5296.6 Hz in both 1H dimensions. Spectra processing and analysis were performed with the Bruker software tools Topspin 1.3 and CCPNMR 2.1.5 (Chignola et al., 2011).

3. Results

3.1. Biological activity of EP-39

First, to characterize EP-39 activity, viral production was evaluated in HEK 293T cells transfected with the HIV-1 pNL4-3 molecular clone. ELISA quantification of CA in culture supernatants after 48 h incubation with 5 µg/ml EP-39 or BVM (Fig. 1A) (no toxicity was observed at these concentrations for EP-39 and BVM. Cytotoxicity in HEK 293T cells are considerably higher than the concentrations used in this assay, 8.5 µM for BVM and 7.9 µM EP-39 respectively) or an equivalent volume of DMSO (the solvent used for the drug resuspension) showed that particle production was slightly reduced (by 18.1%) only in cells exposed to BVM, but not to EP-39, compared with control (DMSO) (Fig. 1B). Electron microscopy (EM) analysis of the shape and size distribution of viral particles produced in control cells (DMSO) showed a very high proportion (~92.9%) of immature and mature typical particles, and also a small fraction (~7.1%) of particles with an acentric core or aberrant immature spherical morphology (Fig. 1C; Supplementary Fig. 1). After incubation with EP-39 or BVM, the proportion of particles with abnormal morphology was significantly increased compared with control (44.2% and 37.3% respectively). The percentage of particles with normal morphology was higher in supernatants from cells exposed to BVM compared with EP-39 (62.7% and 55.8%) (Fig. 1C). In these samples, aberrant mature particles were characterized by acentric cores associated with the persistence of a partial or total spherical shell under the viral membrane, or with roundish masses localized at the center or on one side of the particle. These morphological features are reminiscent of the BVM-generated morphological defects reported by others (Adamson et al., 2006; Keller et al., 2011; Li et al., 2003). These results confirm that EP-39 inhibits CA-SP1 maturation, like the BVM drug lead, generates a slightly higher proportion of aberrant particles, supporting its more effective maturation inhibition.

To analyze the effect of EP-39 on Pr55Gag assembly, HEK 293T cells were transfected with the p55M1-10 plasmid to express full-length wild type (WT) Pr55Gag and induce the formation of Virus-Like Particles (VLPs) (Schneider et al., 1997). EM analysis of VLP morphology after incubation of transfected HEK 293T cells with 5 µg/ml of EP-39, BVM or DMSO for 48 h showed that VLPs produced in DMSO- or EP-39-treated cells were all roughly spherical and with similar size distribution. In BVM-treated cells, some VLPs displayed aberrant immature morphologies (Fig. 1D). This last observation supports the previous finding that exposure to BVM at high concentration affects also particle assembly (DaFonseca et al., 2007; Kanamoto et al., 2001).

3.2. Selection for EP-39 and BVM-resistant HIV-1 isolates in vitro

To identify mutations that confer resistance to EP-39 or BVM, ten flasks of H9-T cells were infected with WT HIV-1 and cultured in the presence of 50 ng/ml EP-39 or BMV. Two additional flaks of non-infected or WT HIV-1 infected cells were cultured without EP-39 or BVM. Genomic DNA was extracted from cells harvested at the peak of p24 production and the Pr55Gag-PR-coding regions were amplified by PCR and sequenced (Figs. 2 and 3). For selection using EP-39, PCR amplification and sequencing allowed the identification of four individual mutations in the CA domain (CA-A194T, CA-T200N, CA-V230I, CA-V230A) and one within SP1 (SP1-A1V) (Fig. 2) and none in PR. No replication was observed for flask number 10 until day 84. The mutations CA-A194T and CA-T200N of two non conserved residues (Li et al., 2013) are both localized in the vicinity of MHR. Previously described mutation conferring resistance to BVM, CA-V230I was detected (Margot et al., 2010; Li et al., 2013). Finally, the SP1-A1V mutation which corresponds to the substitution of the first residue of SP1 conserved in the major subtypes of the HIV-1 group M (subtypes: A1, B, C, D, F1, G and CRF01_AE, CRF02_AG) was the most common, suggesting that this substitution could be detrimental for EP-39 activity. This last mutation was identified in one antiretroviral-experienced patient infected with clade B virus (Seclén et al., 2010). When using BVM for the selection experiment, three mutations in the CA domain (CA-A194T, CA-L231F, CA-L231M) and three within SP1 (SP1-A1V, SP1-S5N and SP1-V7A) (Fig. 3) were identified. The CA-A194T was already identified in our EP-39 *in vitro* selection. Other mutations have been previously described: CA-L231F (Adamson et al., 2006; Zhou et al., 2004) CA-L231M (Adamson et al., 2006) SP1-A1V (Adamson et al., 2006; Li et al., 2003) and SP1-V7A (Adamson et al., 2010; Lu et al., 2011; Margot et al., 2010; Richards and McCallister, 2008; Van Baelen et al., 2009).

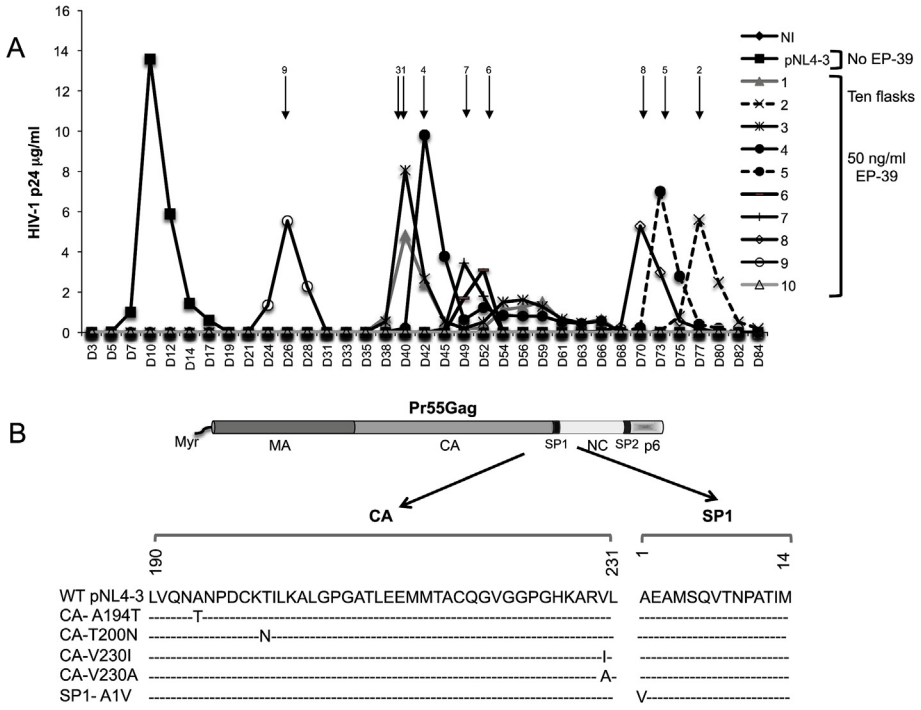

Fig. 2. Selection for EP-39 resistance-inducing mutations. (A) Ten flasks of H9-T cells infected with WT HIV-1 viruses produced in pNL4-3-transfected HEK 293T cells were cultured in the presence of 50 ng/ml EP-39. As controls, two flasks of non-infected (NI) or WT HIV-1-infected cells were cultured without EP-39. Genomic DNA was extracted at peak p24 production (indicated by a narrow) and analyzed by PCR amplification and DNA sequencing. (B) Pr55Gag schematic representation (upper panel). The alignment (lower panel) shows the four resistance mutations in the CA domain and the one in the SP1 domain.

Conversely, the previously described substitutions at positions CA-H226, CA-V230 or SP1-A3 (*in vitro* experiments), or the CA-V230I mutation identified in BVM non-responding patients (Adamson et al., 2006; Margot et al., 2010) were not detected in the present work. The mutations SP1-S5N and SP1-V7A are both localized within SP1 polymorphic motif. As for EP-39, the SP1-A1V mutation was the most common in our experiment. In conclusion, EP-39 or BVM led to some common mutations in resistant HIV-1 viruses (CA-194T, CA-V230I and SP1-A1V), but also to compound-specific substitutions (for EP-39: CA-T200N and CA-V230A, for BVM: CA-H226Y, CA-L231 F/M, SP1-A3V/T, SP1-S5N and SP1-V7A). This suggests that EP-39 and BVM might be involved in slightly distinct contacts in the potential common binding pocket. Moreover, all the data suggest a major role of the first SP1 residue because, when mutated to valine, it can induce resistance to EP-39, BVM and PF-46395, a distinct MI chemical class (Adamson et al., 2006; Waki et al., 2012).

3.3. Replication kinetics of BVM or EP-39-resistant mutants in the presence of EP-39

To compare EP-39 and BVM activities, the replication kinetics of the BVM and EP-39-resistant HIV-1 isolates cloned in pNL4-3 were assessed in infected H9-T cells cultured with/without EP-39 (50 ng/ml and 1 µg/ml). WT HIV-1 replicated with a peak at around 10 days post-infection

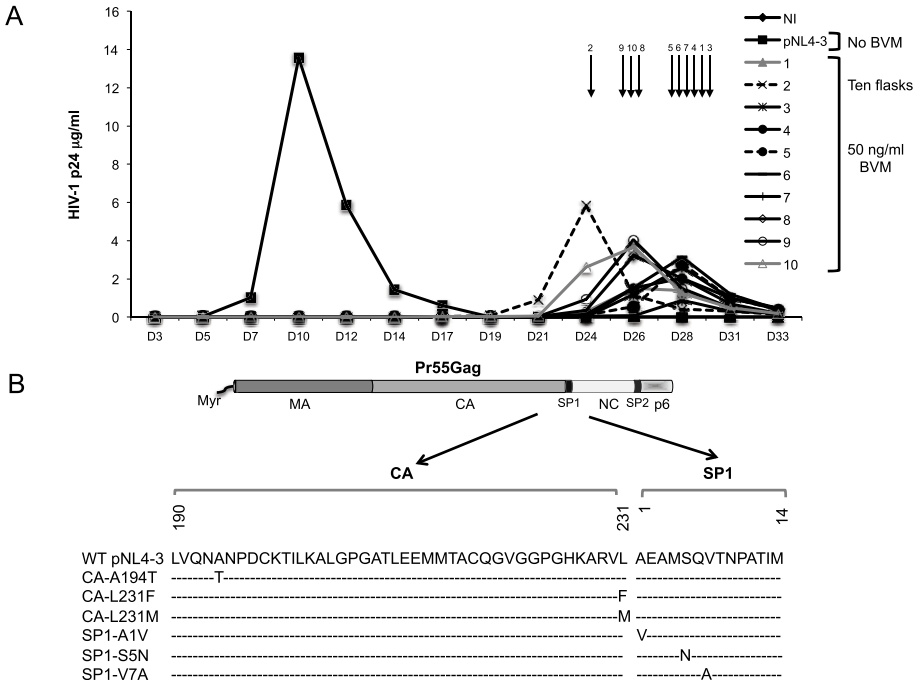

Fig. 3. Selection of BVM resistance-inducing mutations. (A) Ten flasks of H9-T cells infected with WT HIV-1 viruses produced in pNL4-3-transfected HEK 293T cells were cultured in the presence of 50 ng/ml BVM. As controls, two flasks of non-infected (NI) or WT HIV-1-infected cells were cultured without BVM. Genomic DNA was extracted at peak p24 production (indicated by a narrow) and analyzed by PCR amplification and DNA sequencing. (B) Pr55Gag schematic representation (upper panel). The alignment (lower panel) shows the three mutations in the CA domain and the three mutations in the SP1 domain.

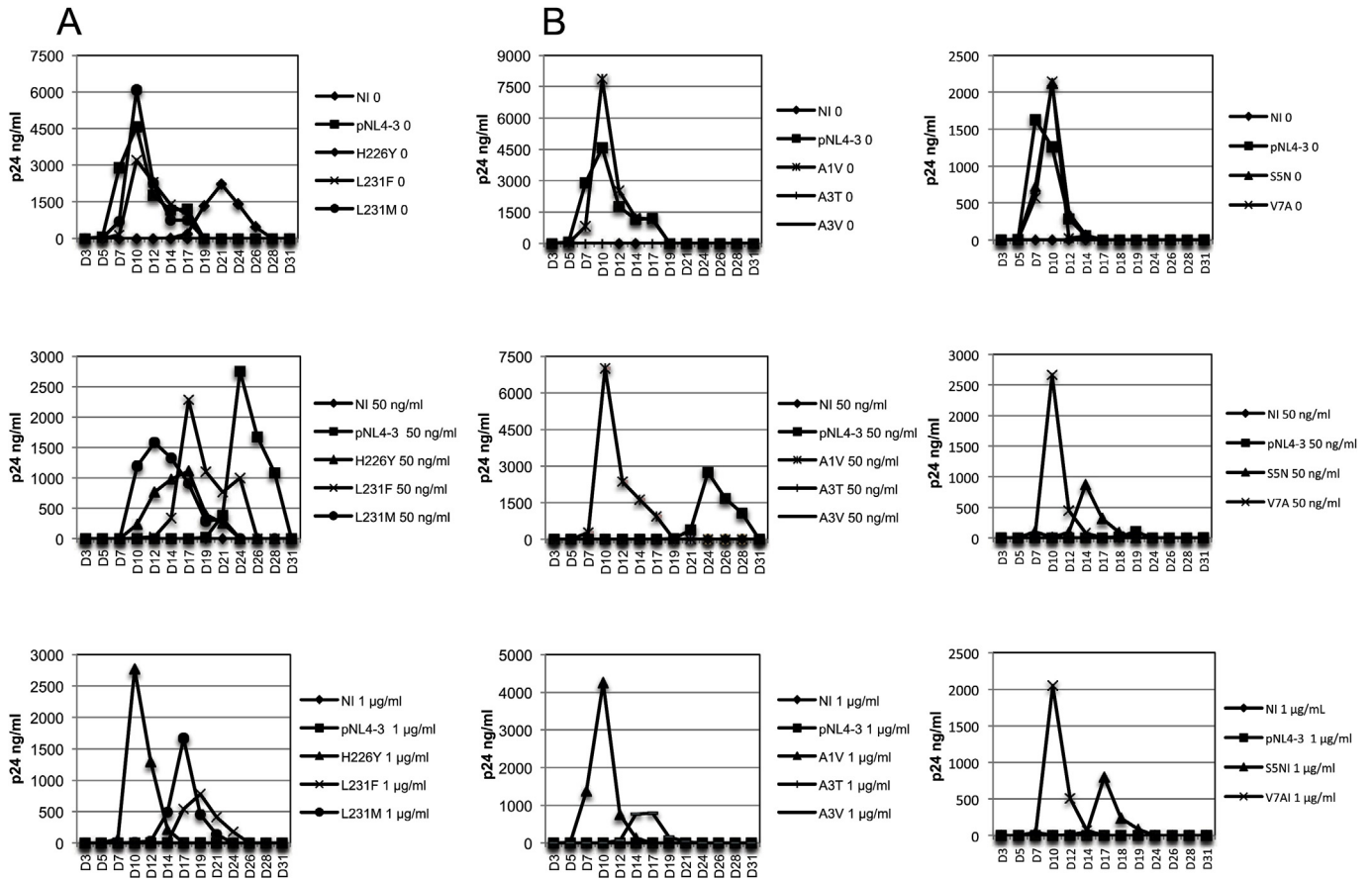

Fig. 4. Replication kinetics of BVM-resistant viruses in the presence or absence of EP-39. H9-T cells were infected with WT or mutant HIV-1 viruses and cultured without or with 50 ng/ml or 1 µg/ml EP-39. Cells were split and supernatants were reserved for HIV-1 p24 quantification by ELISA. Values are the mean ± SD of duplicate experiments. (A) Replication kinetics of viruses with BVM-induced mutations within the CA domain in the presence or absence of EP-39. (B) Replication kinetics of viruses with BVM-induced mutations within the SP1 domain in the presence or absence of EP-39. NI, non-infected cells.

in the absence of EP-39 and at around 20–25 days post-infection in the presence of 50 ng/ml EP-39. No WT HIV-1 virus replication was detected in cells exposed to 1 µg/ml of EP-39 (Figs. 4 and 5). In cells infected with BVM-resistant mutants, four different phenotypes were observed: (i) similar replication kinetics in the presence or absence of 50 ng/ml or 1 µg/ml EP-39 (SP1-A1V and SP1-V7A), demonstrating that these HIV-1 mutants are resistant to BVM and also to EP-39 (Fig. 4). Similar results were obtained for SP1-A1V in SCID-hu Thy/Liv 4892 mice treated with BVM where virus replication was not impaired (Stoddart et al., 2007); (ii) slight replication delay at 50 ng/ml (peak around day 15 post-infection) and 1 µg/ml (peak around day 18 post-infection) for the CA-A194T (common EP-39- and BVM-induced mutation) (Fig. 5), CA-L231F, CA-L231M, and SP1-S5N (Fig. 4) mutant viruses, indicating that they are still sensitive to EP-39; (iii) delayed replication in the absence of EP-39 (peak at day 21 post-infection) and earlier replication peak in the presence of EP-39 (peak at day 17 post-infection with 50 ng/ml and at day 10 post-infection with 1 µg/ml of EP-39) for the CA-H226Y mutant virus (Fig. 4). These results (delayed replication without EP-39) do not appear as pronounced as in the previous published data showing replication in the absence of BVM or PF46396 (Adamson et al., 2006; Waki et al., 2012). As sequencing did not identify any additional mutation in CA-H226Y, we can speculate that this difference could be due to the fact that in our study the replication assays were initiated by infection as opposed to previous studies where the replication assay was initiated by transfection. Our replication kinetic data suggest that EP-39 is able to rescue the assembly/release defects imposed by this mutant; and (iv) no replication (or very slight) in the presence or absence of EP-39. Specifically, for the SP1-A3V mutant a slight replication was observed at day 16 post-infection only after incubation with 1 µg/ml of EP-39, indicating that its defective replication is enhanced by EP-39, as previously described for BVM (Adamson et al., 2006). Conversely, the SP1-A3T mutant did not replicate with or without EP-39 (Fig. 4).

It must be stressed that CA-A194 presents only one possible substitution in most of the HIV-1 isolates of the HIV-1 group M, whereas SP1-S5 and SP1-V7 are highly polymorphic residues. The residues CA-H226, CA-L231, SP1-A1, SP1-A3 are all conserved residues in the HIV-1 group M (Li et al., 2013). Analysis of the replication kinetics of the EP-39 resistant mutants showed that the four CA mutant viruses displayed two distinct phenotypes. CA-A194T and CA-T200N replicated with a slight delay (day 17 post-infection) in the presence of 50 ng/ml and 1 µg/ml EP-39 (Fig. 5), suggesting a residual level of sensitivity. CA-V230I, CA-V230A (Fig. 5) and SP1-A1V (Fig. 4) replicated like WT viruses in the absence and in the presence of 50 ng/ml and 1 µg/ml EP-39, showing that they are resistant to EP-39 even at high concentration. Altogether, these results underline that the SP1-A1V mutation corresponds to the major event in EP-39 resistance development.

3.4. Effect of EP-39- and BVM on the CA-Sp1 processing of the resistant mutants

To assess EP-39 and BVM capacity to disrupt CA-SP1 processing in BVM- and EP-39-resistant mutants viruses, HEK 293T cells were transfected with WT or mutant pNL4-3 clones and cultured in the absence or presence of BVM or EP-39 (0, 1 or 2 µg/ml). Western blotting with an anti-p24 antibody of normalized amounts of cell lysates or

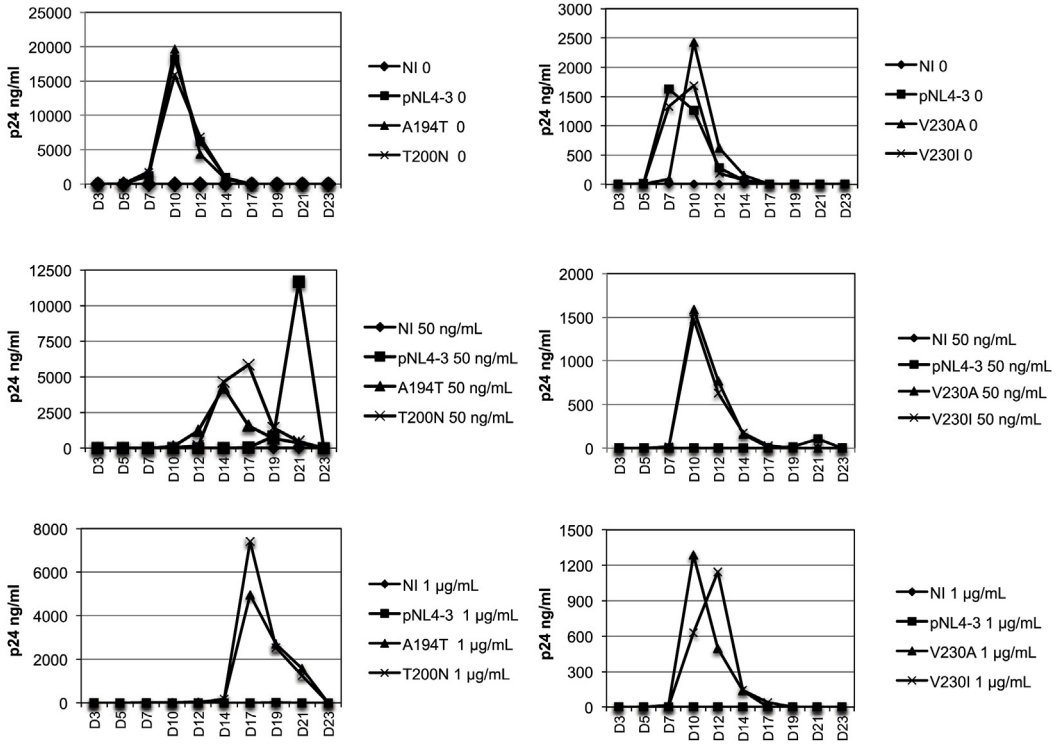

Fig. 5. Replication kinetics of EP-39-resistant viruses in the presence or absence of EP-39. H9-T cells were infected with WT or mutant HIV-1 viruses and cultured without or with 50 ng/ml or 1 µg/ml EP-39. Cells were split and supernatants were reserved for HIV-1 p24 quantification by ELISA (Ingen). Values are the mean ± SD of duplicate experiments. NI, non-infected cells.

sucrose cushion-purified viruses showed that in the presence of EP-39, CA-SP1 accumulated in cell and virus fractions (Supplementary Fig. 2). In the presence of EP-39, CA-SP1 accumulated also in samples from HEK 293T cells transfected with pNL4-3 CA-A194T or SP1-S5N in an EP-39 concentration-dependent manner. This accumulation was less important with the CA-L231F and CA-L231M clones (20% less at 1 µg/ml). These results indicate that these mutations are partially sensitive to EP-39, as shown by us (Fig. 4) and by Adamson et al. using BVM (Adamson et al., 2006). CA-SP1 accumulation in the virus fraction was concentration-dependent also for the SP1-A3V and SP1-A3T mutants. Conversely, with the mutant CA-H226Y, the CA-SP1 level increased in the presence of 1 µg/ml EP-39, and decreased in the presence of 2 µg/ml EP-39. These data suggest that the BVM-resistant mutants CA-H226Y, SP1-A3V and SP1-A3T are EP-39 dependent, as shown by the kinetics experiments (Fig. 4). Analysis of the EP-39-resistant mutant viruses showed that with the CA-T200N virus, CA-SP1 accumulated in the presence of EP-39, indicating that this mutation does not completely restore CA-SP1 processing. The CA-V230A and CA-V230I resistant viruses showed an intermediate sensitivity to EP-39 (1 µg and 2 µg). Finally, analysis of the effect of BVM on EP-39- and BVM-resistant mutant isolates showed that all EP-39-resistant viruses (CA-A194T, CA-T200N, CA-V230A, CA-V230I, SP1-A1V) and also the BVM-resistant viruses SP1-S5N and SP1-V7A were totally resistant to BVM. Altogether, the EP-39- or BVM-resistant viruses do not exactly display the same phenotype when exposed to EP-39 or BVM, reinforcing the idea that these two compounds would not interact in the same way within the binding-pocket.

3.5. EP-39 effect on the particle morphology of BVM- and EP-39-resistant mutants

To investigate the morphology of BVM and EP-39-resistant mutant viruses, HEK 293T cells were analyzed by EM after transfection with WT or mutant molecular clones and incubation or not with EP-39 at 5 µg/ml. WT particles from untreated HEK 293T cells contained condensed conical cores (Fig. 6A, panel a). In contrast, WT particles from EP-39-treated cells (5 µg/ml) displayed acentric and aberrant cores (Fig. 6A, panel b). As CA-L231F, CA-L231M, SP1-A1V and SP1-A3T virus morphologies were described previously (Adamson et al., 2006), this analysis focused on the CA-A194T, SP1-S5N, SP1-V7A, CA-T200N, CA-V230A and CA-V230I mutants. The BVM-resistant viruses CA-A194T, SP1-S5N, SP1-V7A and the EP-39-resistant CA-V230I and CA-V230A mutants presented conical cores, like WT viruses, in the absence of EP-39. Conversely, after incubation with 5 µg/ml EP-39, CA-A194T, SP1-S5N (BVM-resistant) and CA-A194T, CA-T200N, CA-V230A, CA-V230I (EP-39-resistant) viruses exhibited acentric and aberrant cores or the persistence of a partial or total spherical shell under the viral membrane (Fig. 6A). The SP1-V7A virus displayed WT morphology even in the presence of EP-39.

Then, investigation of the morphology of the BVM-resistant CA-H226Y and SP1-A3V viruses in the absence of EP-39 showed that cells infected with the CA-H226Y virus presented most often immature-like particles, some accumulations of Pr55Gag at the plasma membrane, and a very small number of released mature particles with normal or aberrant condensed core (Fig. 6B, panels a–b). In cells infected with SP1-A3V viruses, electron-dense patches of Pr55Gag were detected at the plasma membrane without any evidence of particle release (Fig. 6B, panels e–f). When cells infected with CA-H226Y virus were incubated with 5 µg/ml EP-39, the number of particles containing a normal condensed core increased significantly, although few immature-like particles were still present (panels c–d). Conversely, in the presence of EP-39 (5 µg/ml), SP1-A3V virus particles presented mostly an immature-like morphology and the very few released virions displayed some degree of core condensation (panels g–h). These results indicate that CA-H226, a key residue that stabilizes the assembly unit (Schur et al., 2016), and SP1-A3 play an important role during HIV-1 assembly (Liang et al., 2002). Finally, for the EP-39-dependent viruses, we can speculate that the increase of virus replication at high concentration of EP-39 could be

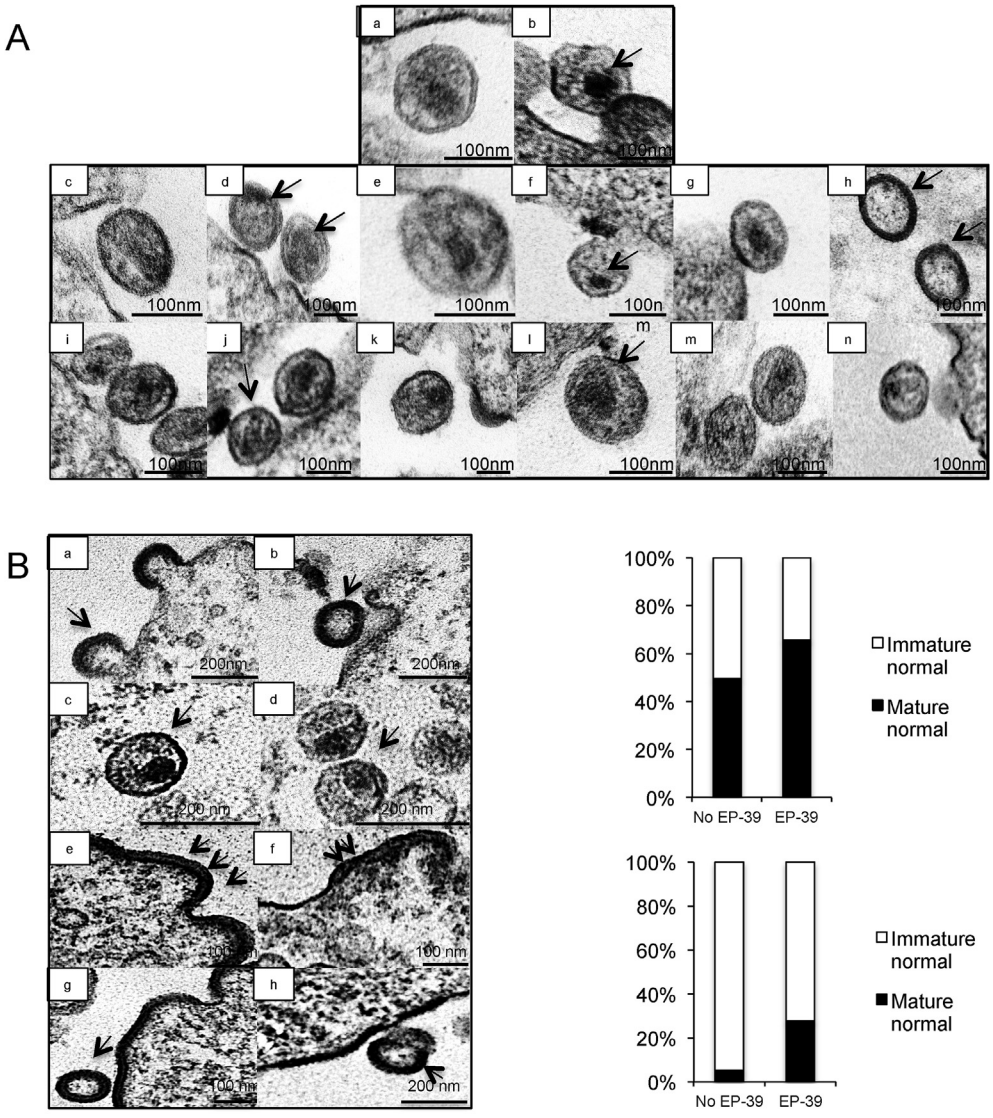

Fig. 6. Morphology of EP-39 and BVM-resistant virus particles. Thin-section EM analysis of WT or mutant virions produced in HEK 293T cells cultured without (DMSO) or with 5.0 µg/ml EP-39. Two days post-transfection, cells were fixed and analyzed by thin-section EM, as previously reported (Brun et al., 2008) (Bar: ≈100 nm). (A) WT HIV-1 virus without (a) and with EP-39 (b); CA-A194T without (c) and with EP-39 (d); CA-T200N without (e) and with EP-39 (f); CA-V230I without (g) and with EP-39 (h); CA-V230A without (i) and with EP-39 (j); SP1-S5N without (k) and with EP-39 (l); SP1-V7A without (m) and with EP-39 (n). (B) Thin-section EM analysis of virions harboring the CA-H226Y or SP1-A3V mutation produced in HEK 293T cells cultured without (a-b and e-f, respectively) or with 5 µg/ml EP-39 (c-d and g-h, respectively). Bar graphs show the ratio of released virions with immature morphology and mature morphology (n = 100–140).

linked to EP-39 capacity to interact with the binding pocket, and also to restore assembly and consecutively the maturation step.

3.6. Assembly properties of EP-39- and BVM-resistant mutants

To further define the effect of EP-39- and BVM-resistant mutations on particle assembly, HEK 293T cells were transfected with WT or mutants cloned in p55M1-10 (Schneider et al., 1997). Then, EM analysis shows that the morphology of the produced VLPs (Fig. 7 and Table 1) using Pr55Gag-CA-A194T (panels c–d), Pr55Gag-CA-T200N (panels e–f), Pr55Gag-CA-V230A (panels i–j), Pr55Gag-CA-V230I (panels k–l) and Pr55Gag-SP1-V7A (panels y–z) was indistinguishable from that of WT particles (panels a–b). The observation of VLPs produced using Pr55Gag-CA-L231F (panels m–n), Pr55Gag-CA-L231M (panels o–p), Pr55Gag-SP1-A1V (panels q–r) and Pr55Gag-SP1-S5N (panels w–x) reveals mixed phenotypes: WT VLPs, aberrant VLPs and also membrane accumulation. Furthermore, in some cells transfected with Pr55Gag-SP1-S5N, VLP budding was affected. Indeed, some VLPs were almost tethered to each other in long chains at the membrane surface. Residues L231 and SP1-A1 are conserved amino acids, which have been proposed to be involved in HIV-1 assembly (Li et al., 2013; Liang et al., 2002). In cells transfected with Pr55Gag-CA-H226Y (panels g–h) a more drastic effect on VLPs phenotype has been detected: some VLPs had a WT phenotype but some possessed an aberrant morphology. Protuberant tubular structures were observed in the supernatant), few accumulations of CA-H226Y at the plasma membrane were also observed. These data confirm that residue H226, an amino acid conserved in all the eight major subtypes of group M (Li et al., 2013), plays a significant role in the assembly of HIV-1 particles (Guo et al., 2005; Liang et al., 2002). In cells transfected with Pr55Gag-SP1-A3V (panels s–t), WT VLPs were very rare, and large electron-dense plaques were detected underneath the plasma membrane. Finally, Pr55Gag-SP1-A3T (panels u–v) strongly accumulated at the plasma membrane and some tubular structures were observed in the supernatant, almost no VLP were detected in the supernatant (data not shown) (Accola et al., 1998; Gross et al., 2000; Kräusslich et al., 1995). These data demonstrate that some EP-39- or BVM-induced substitutions of non-conserved residues in Pr55Gag have no or little direct effect on the assembly step, as indicated by the mild consequences on VLP morphology. Other mutations (CA-H226Y and SP1-A3, two conserved residues) strongly affected VLP morphology, confirming their crucial role in the assembly step (Liang et al., 2002) (Fig. 7, panels g–h and 8 s-v). These data seem to be in agreement with the replication defects of the CA-H226Y, SP1-A3V and SP1-A3T mutant viruses. Next, we quantified VLP release. Supernatant of HEK 293T cells transfected with WT or mutant Pr55Gag plasmids (Supplementary Fig. 3) were subjected to sucrose cushion ultracentrifugation. VLPs released in the medium and Pr55Gag protein expression in the cells were analyzed by Western blot. The relative VLPs

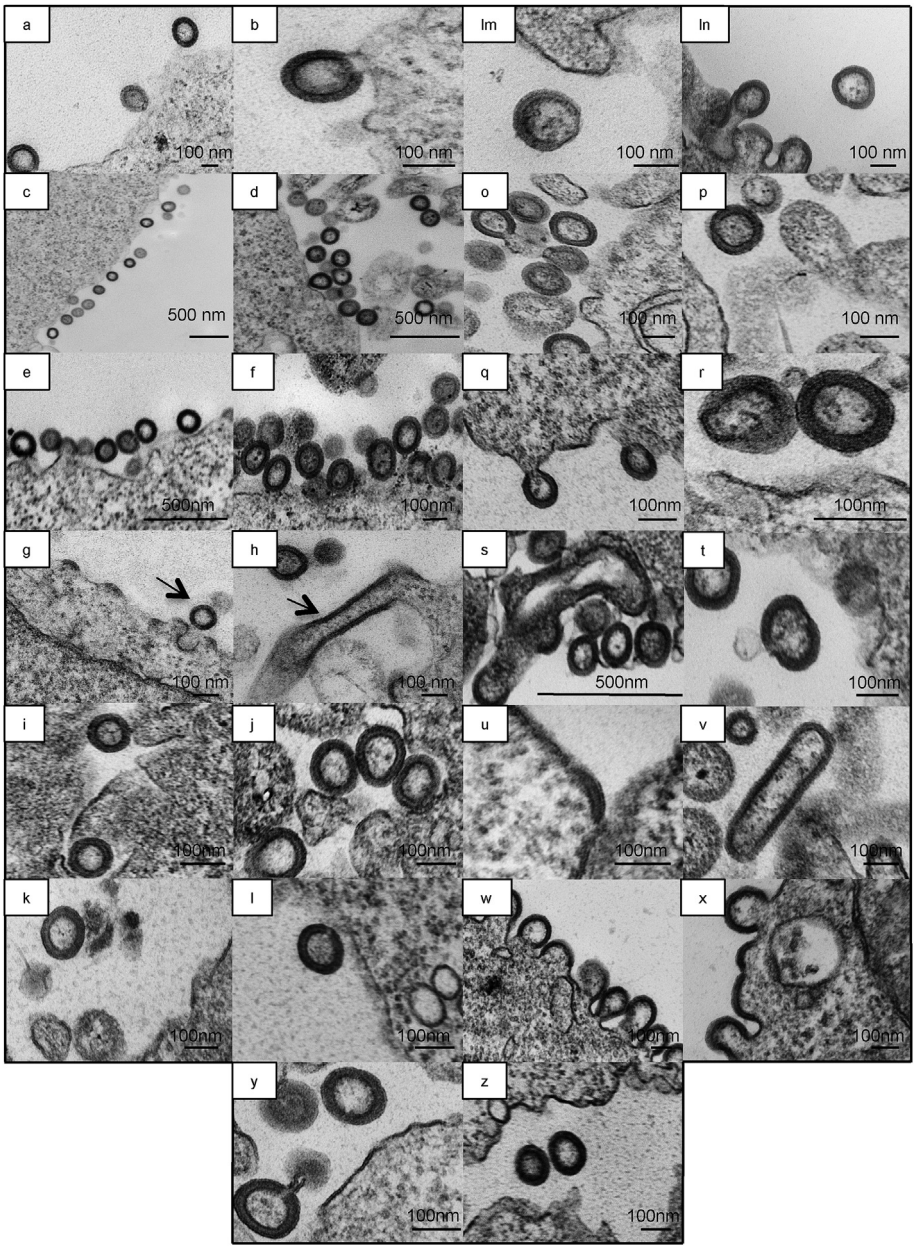

Fig. 7. Assembly of Pr55Gag mutants. Each EP-39 and BVM-induced mutation was introduced in the pCMV55M1-10 plasmid to generate Pr55Gag CA-A194T, CA-T200N, CA-H226Y, CA-V230A, CA-V230I, CA-L231F, CA-L231M, SP1-A1V, SP1-A3V, SP1-A3T, SP1-S5N and SP1-V7A. Thin-section EM images of HEK 293T cells after transfection with the indicated Pr55Gag expression plasmids: WT (a,b); CA-A194T (c,d); CA-T200N (e,f); CA-H226Y (g,h); CA-V230A (i,j); CA-V230I (k,l); CA-L231F (m,n); CA-L231M (o,p); SP1-A1V (q,r); SP1-A3V (s,t); SP1-A3T (u,v); SP1-S5N (w,x); and SP1-V7A (y,z). Bar: ≈100 nm or 500 nm.

release efficiency was determined as the amount of released Pr55Gag (VLPs) normalized to Pr55Gag cell expression levels. The quantity of VLPs generated by the Pr55Gag mutants CA-A194T, CA-H226Y, CA-V230A, CA-V230I, CA-L231M, SP1-A1V, SP1-S5N and SP1-V7A was comparable or sometimes higher to WT VLPs. Conversely, the amount of VLPs formed by the Pr55Gag mutants CA-T200N, CA-L231 was slightly reduced while that of VLPs formed by the Pr55Gag mutants SP1-A3V and SP1-A3T mutants was severely decreased (Supplementary Fig. 3). Together, these observations demonstrate that the CA-H226Y mutation causes a morphological defect of VLPs, but no defect in particle release, while SP1-A3V and SP1-A3T lead to a strong accumulation of Pr55Gag at the plasma membrane and the production of very few VLPs.

3.7. *In silico docking of EP-39 and BVM on the hexameric crystal structure of the CA_{CTD}-SP1 Gag fragment*

The results obtained using EP-39- and BVM-induced mutants suggested that these MIs might share the same binding pocket but interact differently in the CA_{CTD}-SP1 hexameric structure. To address this hypothesis, *in silico* docking of EP-39 and BVM on the hexameric crystal structure, PDB ID 5I4T (Wagner et al., 2016), was performed using the GOLD docking program (Jones et al., 1995, 1997). For both ligands all poses were located inside the goblet-shaped hexamer with different position or orientation. Essentially due to a larger contribution of hydrogen bonds in the case of EP-39, the scores for EP-39 (25.1–25.4) were systematically better than those for BVM (22.4–22.9). Nevertheless for both, the ten best poses could be clustered in two groups with comparable scores, but different orientations. In group I, EP-39

Table 1
Phenotypes of Pr55Gag virus-like particles (VLPs) derived from wild-type Pr55Gag or mutant Pr55Gag expression.

WT (aa)	Mutant (aa)	Particle morphology	Reference
Capsid			
A194	T	Proper spherical VLPs	This report
T200	N	Proper spherical VLPs Few released VLPs	This report
H226	Y	Proper spherical VLPs Aberrant VLPs Some membrane accumulation and tubes at the surface of plasma membrane (PM)	This report[a]
V230	A	Proper spherical VLPs	This report
V230	I	Proper spherical VLPs	This report
L231	F	Proper spherical VLPs Aberrant VLPs	This report
L231	F	Proper spherical VLPs Aberrant VLPs	This report
SP1			
A1	V	Proper spherical VLPs Rare aberrant VLPs Little membrane accumulation	This report[b]
A3	V	Rare proper spherical VLPs Many aberrant VLPs Membrane accumulation	This report[b]
A3	T	Strong membrane accumulation, Tubes at the surface of PM.	This report[c]
S5	N	Proper spherical VLPs Aberrant VLPs Minimal membrane accumulation	This report
V7	A	Proper spherical VLPs	This report

[a] Results reported previously (Liang et al., 2002).
[b] Results reported previously (Liang et al., 2002; Adamson et al., 2006).
[c] Results reported previously (Adamson et al., 2006; Datta et al., 2011).

and BVM (Fig. 8) show molecular interactions within the lower part of the barrel formed by the 6-helix bundle stem and were in contact with up to all six chains of the hexamer. Poses were, for both ligands, in close contact with conserved residues: CA-K158 in the MHR, CA-G222, CA-G223 (only for EP-39) and CA-P224 in the GVGGP β-turn motif (CA-VGG hinge and the CA-P224), CA-K227 and CA-L231 in CA C-terminus, and SP1-M4 (Li et al., 2013). EP-39 and BVM establish respectively two and one hydrogen bonds with the hexamer (Supplementary Figs. 4A and B). The common hydrogen bond involved the carbonyl in position C-28 and the ε-amino of CA-K158 of the monomer chain i. The additional hydrogen bond specific to EP-39 involved the amino group at position C-28 with the backbone carbonyl of CA-G222 in the GVGGP β-turn motif of monomer k (Supplementary Fig. 4A). This amino group was around 3 Å from the ε-amino of both CA-K158 of monomer j in the MHR region and CA-K227 of the same monomer. For BVM, an additional location within the barrel was observed (Fig. 8) that resulted from a sliding of BVM of nearly 7 Å into the SP1 side of the 6-helix bundle stem. The hydrogen bond was lost, whereas new contacts were established with CA-L231 and SP1-M4 of all monomers. These computational results are in agreement with experiments showing that a BVM derivative harboring in position C-28 a photoactivable group crosslinks to both the junction helix and the MHR domain (Nguyen et al., 2011), and also with a NMR, cryo-EM and molecular dynamics simulation study suggesting an interaction between SP1 and MHR (Wang et al., 2017). In group II, EP-39 and BVM (Fig. 8) revealed interactions with the upper part of the goblet-shaped hexamer and spread out along the interface between the MHRs of two consecutive chains. Substituent at C28 position in group II poses maintained the contacts and interactions observed in group I. Particularly, the EP-39-specific hydrogen bond involving the amino group at position C-28 with the backbone carbonyl of CA-G222 was still observed (Supplementary Fig. 4C). Contrarily from group I, the C-28 side was almost perpendicular to the barrel, on the platform made with CA-K227 of the i and i + 1 chains, while the C-3 side slid into a cleft delineated by the conserved amino acids of chain i MHR (CA-G156:CA-E159) on one side, and the conserved amino acid of chain i + 1 MHR (CA-K158:CA-R162) on the other side. The group at position C-3 could be involved in three possible hydrogen bonds (only two simultaneously) with the side chains of CA-R162 and CA-D163 (chain j) and the amide nitrogen of CA-K158 (chain i) (Supplementary Figs. 4C and D). As it has been previously shown for the BVM (Nguyen et al., 2011), it seems that EP-39 may engage contacts in this highly conserved motif that is found within the Gag protein of all *orthoretroviruses* (Tanaka et al., 2016) and is critical for HIV-1 assembly. Moreover, our computational analysis revealed that EP-39 and BVM could establish contacts and/or hydrogen bonds with conserved

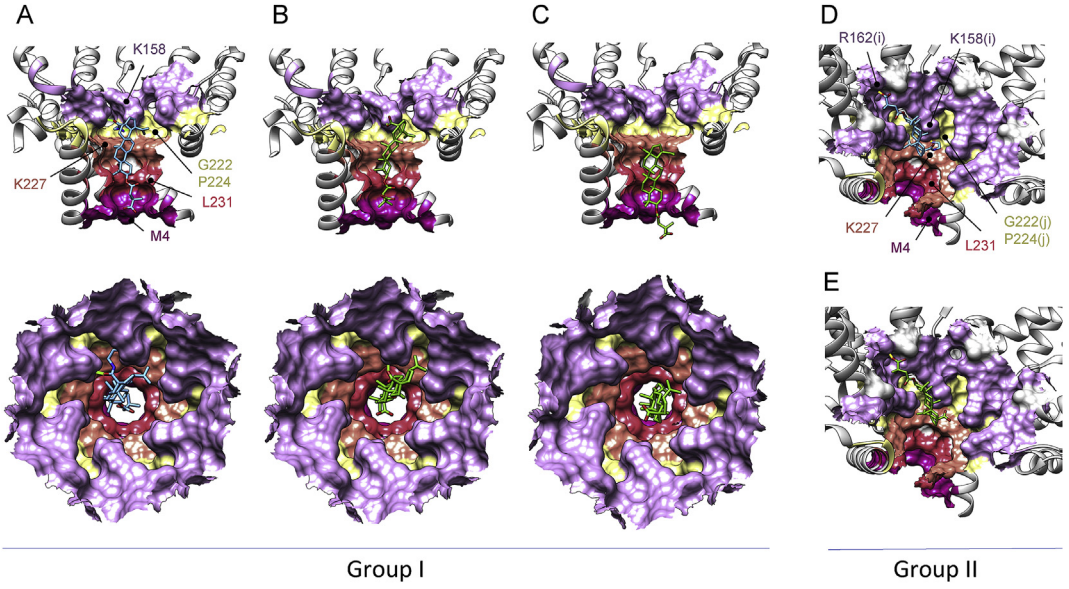

Fig. 8. *In silico* docking of EP-39 and BVM on the hexameric crystal structure of the CA_{CTD}-SP1 Gag fragment. Radial and axial views of the binding of EP-39 (A) and BVM (B) within the lower part of the barrel formed by the 6-helix bundle stem (Group I). They are both in contact with up to all six chains of the hexamer. An additional location, within the barrel, is observed for BVM (C) resulting from sliding to the SP1 side. In this case, proximities with CA-K158, the CA-G222-CA-P224 stretch and the hydrogen bond are lost. New contacts are established with CA-L231 and SP1-M4. In group II, EP-39 (D) and BVM (E) interact with the upper part of the goblet-shaped hexamer and spread out along the interface between the MHRs of two consecutive chains.

residues located in the three parts of the "assembly unit" (Schur et al., 2016). Mutation into alanine of these residues abolishes virus assembly (Melamed et al., 2004; von Schwedler et al., 2003). Together these results confirm that the modification introduced at C-28 increases EP-39 binding and positioning on the target and also improves its MI activity. These data reinforce the hypothesis previously put forward that MI activity is linked to their ability to stabilize the Pr55Gag lattice through binding to the barrel formed by the 6-helix bundle, and then to reduce the cleavage at the CA-SP1 junction that remains inaccessible. Moreover, we can speculate that resistance-inducing mutations counteract MI stabilization by inducing a conformational change, allowing access by the protease to the cleavage site at the CA-SP1 junction.

3.8. NMR analysis of the CA-SP1-NC domain interacting with EP39

The recent atomic model of the HIV-1 CA-SP1 region in the immature arrangement describes a set of complex intra- and inter-molecular interactions essential for the assembly of immature HIV-1 particles and delineates the assembly unit that defines the hexamer structure (Schur et al., 2016; Wagner et al., 2016). The first demonstration of a direct interaction between BVM and its target Pr55Gag was obtained by using photoaffinity analogs of BVM (46). To determine the interactions between MIs and Pr55Gag, solid phase chemistry was used to synthesize the wild type peptide (CA-SP1-NC) that contains SP1 (1-14) surrounded by CA C-terminus (190-231) and NC N-terminus (1-13) (total length: 48 amino acids), and the mutant (CA-SP1(A1V)-NC) that harbors A1V, the most common mutation in EP-39 and BVM selected isolates. The structures of the wild type peptide (CA-SP1-NC) (Morellet et al., 2005) and the structure of the mutant (CA-SP1(A1V)-NC) (to be published) were studied by NMR. It is important to note that the sequence of the CA-SP1-NC domain used in our NMR study is different from the one used for the mutation experiments. Specifically, a serine at position 10 (POL_HV1LW) within SP1 in the NMR study was replaced by a proline (POL_HVIN5) in the sequence used for the mutation study. This substitution should not be crucial because this part of the domain is not well conserved and this residue does not affect virus replication. As this peptide has a strong tendency to aggregate in 100% H_2O, the working solution contained 30% trifluoroethanol (TFE), a hydrophobic solvent, to favor solubilization (Morellet et al., 2005). Moreover, only EP-39 was used because it is more hydrosoluble than BVM. The 2D ^1H-^1H NOESY experiments with CA-SP1-NC (Fig. 9A) and CA-SP1(A1V)-NC (Fig. 9B) in the presence or not of EP-39 and the chemical shift perturbations caused by EP-39 (Fig. 9C and D) showed that although some perturbed amino acids were located in the CA portion (CA-M215, CA-G222), at the end of the SP1 domain (SP1-I13, SP1-M14) and in the NC domain (NC-MQR1-3, NC-KI11-12), the most perturbed amino acids were mainly in the SP1 domain (SP1-A1 to SP1-N9). When using CA-SP1 (A1V)-NC, addition of EP-39 caused only one major perturbation at SP1-A3. The perturbation of CA-E212, CA-E213 and NC-V13 located at the extremities of the peptide were not meaningful (Fig. 9B). These first NMR data for a MI clearly show that the modification induced by the mutation SP1-A1V (induced by BVM and also EP-39) fully inhibits EP-39 binding. This mutation does not allow EP-39 binding to its drug-binding pocket and allows the cleavage at the CA-SP1 junction by the PR, suggesting a close relationship between MI anti-HIV-1 activity and their capacity to bind to CA-SP1. Indeed, it has been recently shown that BVM and its derivatives bind to and perturb the conformation of the CA–SP1 junction (Wang et al., 2017).

4. Discussion

In the current study, we extended our earlier analysis on EP-39, a BVM-derivative (Coric et al., 2013). No studies were ever conducted to identify the mutations generated by EP-39, to determine its mode of action and to compare it to that of BVM. First, we demonstrated that EP-39 does not affect virus particle production, but efficiently inhibits CA-SP1 processing of HIV-1 and leads to higher production of abnormal viruses. We identified six mutations induced by BVM: CA-194T, CA-L231 M/F, SP1-A1V, SP1-S5N and SP1-V7A a mutation of the highly polymorphic amino acid located in the SP1 QVT motif that was previously detected in patients resistant to BVM (Wang et al., 2015). *In vitro* selection using EP-39 identified five mutations: CA-A194T, CA-T200N, CA-V230I/A and SP1-A1V. Altogether, these data show that these two compounds induced common but also compound-specific mutations to escape the selection pressure. This suggests that although these two molecules share a common chemical skeleton, the additional chemical modification (C-28 for EP-39) could induce a different interaction with Pr55Gag and this could explain the appearance of compound-specific mutants. The characterization of the BVM- and EP-39-resistant mutant viruses using replication kinetics, biochemical assays and EM in the presence of BVM or EP-39 comforts this hypothesis. Indeed, some BVM-resistant mutant viruses presented the same phenotype in the presence of BVM or EP-39. Altogether, our results show that EP-39 and BVM induce common and divergent resistance mutations that are localized around the CA-SP1 cleavage site and in the SP1 domain and that concern polymorphic or conserved residues. The induced mutations can be classified in two groups: (i) mutations on conserved and polymorphic amino acids that destabilize the immature lattice with no or little impact on viral assembly and (ii) mutations on conserved residues with a strong negative effect on virus assembly. In this second group, we can hypothesize that the MI stabilization properties compensate for the profound destabilization effect on the immature lattice organization and restore viral particle assembly and sometimes also maturation. In the presence of EP-39, the number of immature particles was strongly increased for the SP1-A3V mutant virus, while the number of mature particles was significantly higher for the CA-H226Y virus. At this stage, we propose that binding of EP-39 rescues the multimerization defect of the CA-H226Y virus, possibly by correcting the impaired folding induced by these mutations, as previously shown for the CA-P224A mutant virus with BVM (Timilsina et al., 2018). These results indicate that EP-39 and BVM induce common and distinct mutations and three distinct phenotypic groups of mutated viruses: mutant viruses with partial sensibility to BVM or EP-39, MI-dependent viruses, and MI-resistant viruses. *In silico* docking of EP-39 and BVM strongly suggested the presence of two binding sites in the immature CA_{CTD}-SP1 Gag fragment that involve regions important for structure stability. Moreover, EP-39/BVM binding is expected to stabilize the hexameric structure and particularly the immature CA lattice, preventing the mature capsid formation (Keller et al., 2011). *In silico* docking also suggested that EP-39 and BVM may engage interactions and/or hydrogen bonds with conserved residues located in the three parts of the hexameric assembly unit (Schur et al., 2016): the CA_{CTD}, the VVG hinge (CA-221 to 223), and the CA-SP1 helix. Specifically, we observed potential contacts with CA-P224 that together with CA-D197 and CA-H226 is involved in a three-way linkage between two neighboring CA-SP1 helices and the base of the CA_{CTD}. This could explain the EP-39-dependence of the CA-H226Y mutant virus. In this mutant, binding to the CA-P224 residue could compensate for the destabilization effect of the CA-H226Y mutation. The *in silico* docking analysis also suggested that interactions are stronger for EP-39 thanks to the additional hydrogen bond with the backbone carbonyl of G222 in the GVGGP β-turn. This interaction through the second hydrogen bond might act as a hinge between the MHR and barrel locations, ensuring a stronger interaction of EP-39 with the hexameric structure. On the other hand, BVM loses contact with the MHR-K158 region and sinks deeper than EP-39 in the barrel. The hydrogen bond is no longer detectable between BVM and the barrel hexameric structure. This is in line with the BVM-specific SP1-S5N and SP1-V7A mutations and is expected to strongly stabilize the 6-helix bundle (Keller et al., 2011). The BVM-specific CA-L231F mutation inhibits BVM binding to the inner part of the barrel.

Finally, NMR data using the more hydrosoluble EP-39 and the peptide CA-SP1-NC showed that the most perturbed amino acids were

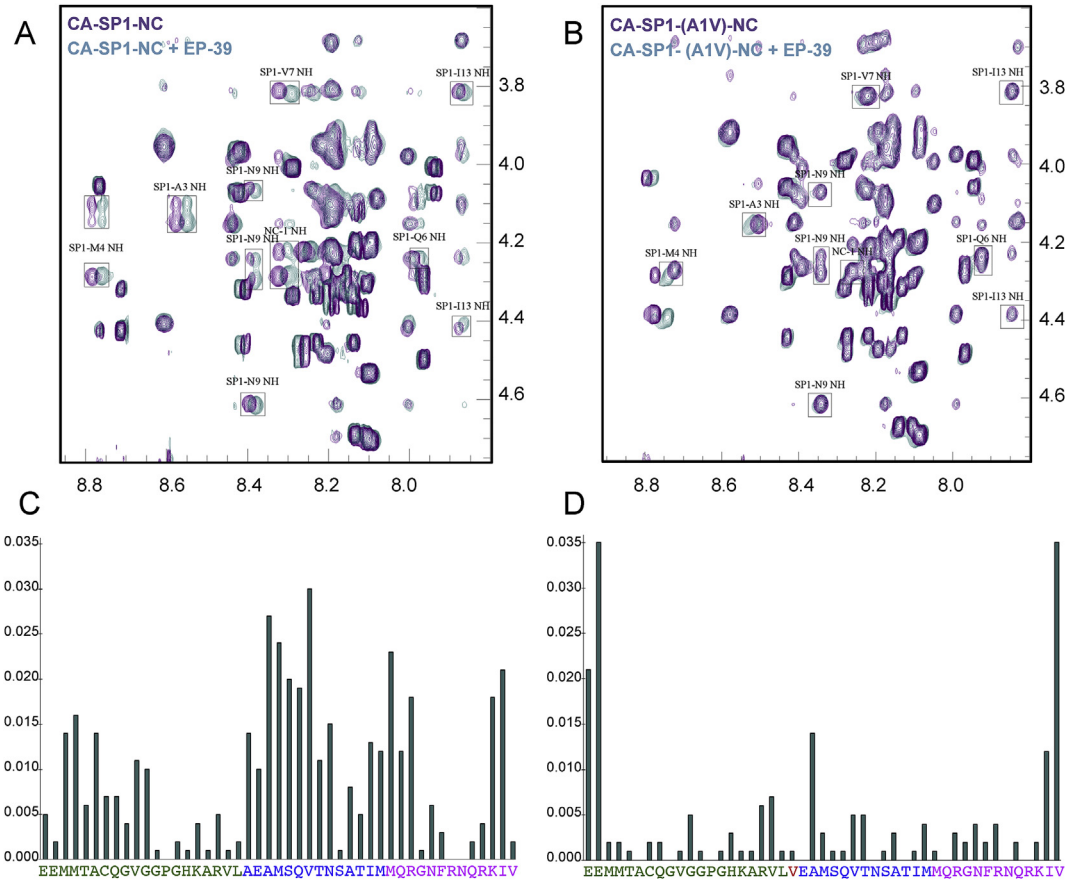

Fig. 9. NMR analysis of the interaction between the maturation inhibitor EP-39 and WT CA-SP1-NC or mutated CA-SP1(A1V)-NC. 2D 1H-NOESY experiments using wild type CA-SP1-NC (A) or mutated CA-SP1(A1V)-NC (B) in the absence (magenta) or presence (cyan) of EP-39. The chemical shift perturbations can be observed on the spectra and the involved residues are indicated. (C and D) The histograms show the chemical shift perturbations caused by addition of EP-39. The interaction of EP-39 is stronger with CA-SP1-NC (C) than with CA-SP1(A1V)-NC. The most perturbed amino acids are located in the SP1 domain and in CA 215-223.

located between SP1-A1 and SP1-N9. Importantly, when using the mutated peptide CA-SP1(A1V)-NC, no specific perturbation was detected. NMR and *in silico* docking results allowed identifying the Pr55Gag residues within the maturation inhibitor-binding pocket that directly interact with EP-39. Moreover, our data confirm the proposed model in which MIs inhibit the maturation step by associating with the interacting site formed by oligomerization of Pr55Gag during the assembly step of HIV-1 particles. According to this model, the antiviral effect of MIs is linked to their capacity to stabilize the immature Gag lattice. Altogether, our findings suggest that MIs could disrupt CA-SP1 processing by PR through restriction of the conformational flexibility around the CA-SP1 junction. Structural studies data indicate that the CA-SP1 cleavage site is hidden within this 6-helix bundle and inaccessible to the PR. MI binding may rigidify the 6-helix structure and reduce the propensity for unraveling and exposure of the cleavage site. Resistance mutations could increase the cleavage site presentation and possibly, as shown for the SP1-A1V mutation and EP-39, prevent MI binding. Finally, our data confirm that EP-39 may exhibit a different binding affinity and positioning on its target and also higher MI activity. The ability of second-generation MIs to induce greater protection from cleavage of polymorphs could be explained by the presence of additional binding contacts within the Pr55Gag. We can speculate that this higher potential binding could lead to a greater stabilization of the Pr55Gag lattice by perturbing molecular motions (Wang et al., 2017), thus rendering the system less sensitive to PR recognition/cleavage.

All our investigations highlighted the importance of the SP1-A1 residue. The mutation SP1-A1V could generate a conformational change that exposes more efficiently the CA-SP1 cleavage site to the HIV-1 protease. The CA-SP1-NC domain structure containing this mutation is in progress to determine its effect on the structure. Alternatively, the A1V substitution could disturb MIs binding capacity and therefore their activities. Moreover, future analyses of BVM derivative should take into account other CA residues and not only the QVT polymorphism. For example, the isoleucine substitution at position CA-V230 is found in the eight major subtypes of the HIV-1 group M and in five patients without natural polymorphisms at the position QVT, suggesting that natural genetic variations conferring resistance to BVM exist beyond these three residues (Margot et al., 2010).

MIs targeting CA-SP1 cleavage represent a very promising, and clinical trials with second-generation maturation inhibitors are underway. Mutants resistant to these MIs, as the EP-39, provide valuable insights into the role of CA-SP1 in HIV-1 assembly and maturation, but also on the mutations in HIV-1 Pr55Gag that render viruses non-responsive to second-generation MIs. Immediate needed is to further identified precisely the binding pocket of the MI and its target using higher resolution approaches are needed to better define the molecular basis for MI activity as well as to conduct a rational-based design of new MIs with improved potency and breadth of antiviral activity. Our NMR studies are a first step in this direction. While further work is clearly needed to fully understand MI activities, the approach described should prove useful to improve MI potency and coverage.

Funding

This work was supported by the CNRS, the University of Montpellier, the Agence Nationale de Recherche sur le SIDA et les hépatites virales (ANRS) and the University of Paris Descartes. The funders had no role in study design, data collection and analysis,

decision to publish, or preparation of the manuscript.

Acknowledgments

We thank Eric Freed and Barbara Felber for kindly providing reagents.

Appendix A. Supplementary data

Supplementary data to this article can be found online at https://doi.org/10.1016/j.antiviral.2019.02.014.

References

Accola, M.A., Höglund, S., Göttlinger, H.G., 1998. A putative alpha-helical structure which overlaps the capsid-p2 boundary in the human immunodeficiency virus type 1 Gag precursor is crucial for viral particle assembly. J. Virol. 72, 2072–2078.

Adamson, C.S., Ablan, S.D., Boeras, I., Goila-Gaur, R., Soheilian, F., Nagashima, K., Li, F., Salzwedel, K., Sakalian, M., Wild, C.T., Freed, E.O., 2006. In vitro resistance to the human immunodeficiency virus type 1 maturation inhibitor PA-457 (Bevirimat). J. Virol. 80, 10957–10971. https://doi.org/10.1128/JVI.01369-06.

Adamson, C.S., Sakalian, M., Salzwedel, K., Freed, E.O., 2010. Polymorphisms in Gag spacer peptide 1 confer varying levels of resistance to the HIV- 1 maturation inhibitor bevirimat. Retrovirology 7, 36. https://doi.org/10.1186/1742-4690-7-36.

Briant, L., Chazal, N., 2011. HIV-1 assembly, release and maturation. World J. AIDS 1, 111–130. https://doi.org/10.4236/wja.2011.14017 Published Online Decem ber 2011.

Briggs, J.A.G., Kräusslich, H.-G., 2011. The molecular architecture of HIV. J. Mol. Biol. 410, 491–500. https://doi.org/10.1016/j.jmb.2011.04.021.

Brun, S., Solignat, M., Gay, B., Bernard, E., Chaloin, L., Fenard, D., Devaux, C., Chazal, N., Briant, L., 2008. VSV-G pseudotyping rescues HIV-1 CA mutations that impair core assembly or stability. Retrovirology 5, 57. https://doi.org/10.1186/1742-4690-5-57.

Checkley, M.A., Luttge, B.G., Soheilian, F., Nagashima, K., Freed, E.O., 2010. The capsid-spacer peptide 1 Gag processing intermediate is a dominant-negative inhibitor of HIV-1 maturation. Virology 400, 137–144. https://doi.org/10.1016/j.virol.2010.01.028.

Chignola, F., Mari, S., Stevens, T.J., Fogh, R.H., Mannella, V., Boucher, W., Musco, G., 2011. The CCPN Metabolomics Project: a fast protocol for metabolite identification by 2D-NMR. Bioinformatics 27, 885–886. https://doi.org/10.1093/bioinformatics/btr013.

Coric, P., Turcaud, S., Souquet, F., Briant, L., Gay, B., Royer, J., Chazal, N., Bouaziz, S., 2013. Synthesis and biological evaluation of a new derivative of bevirimat that targets the Gag CA-SP1 cleavage site. Eur. J. Med. Chem. 62, 453–465. https://doi.org/10.1016/j.ejmech.2013.01.013.

DaFonseca, S., Blommaert, A., Coric, P., Hong, S.S., Bouaziz, S., Boulanger, P., 2007. The 3-O-(3',3'-dimethylsuccinyl) derivative of betulinic acid (DSB) inhibits the assembly of virus-like particles in HIV-1 Gag precursor-expressing cells. Antivir. Ther. (Lond.) 12, 1185–1203.

Dang, Z., Ho, P., Zhu, L., Qian, K., Lee, K.-H., Huang, L., Chen, C.-H., 2013. New betulinic acid derivatives for bevirimat-resistant human immunodeficiency virus type-1. J. Med. Chem. 56, 2029–2037. https://doi.org/10.1021/jm3016969.

Datta, S.A.K., Temeselew, L.G., Crist, R.M., Soheilian, F., Kamata, A., Mirro, J., Harvin, D., Nagashima, K., Cachau, R.E., Rein, A., 2011. On the role of the SP1 domain in HIV-1 particle assembly: a molecular switch? J. Virol. 85, 4111–4121. https://doi.org/10.1128/JVI.00006-11.

Dunbrack, R.L., 2002. Rotamer libraries in the 21st century. Curr. Opin. Struct. Biol. 12, 431–440.

Freed, E.O., 2015. HIV-1 assembly, release and maturation. Nat. Rev. Microbiol. 13, 484–496. https://doi.org/10.1038/nrmicro3490.

Fujioka, T., Kashiwada, Y., Kilkuskie, R.E., Cosentino, L.M., Ballas, L.M., Jiang, J.B., Janzen, W.P., Chen, I.S., Lee, K.H., 1994. Anti-AIDS agents, 11. Betulinic acid and platanic acid as anti-HIV principles from Syzygium claviflorum, and the anti-HIV activity of structurally related triterpenoids. J. Nat. Prod. 57, 243–247.

Ganser-Pornillos, B.K., Yeager, M., Pornillos, O., 2012. Assembly and architecture of HIV. Adv. Exp. Med. Biol. 726, 441–465. https://doi.org/10.1007/978-1-4614-0980-9_20.

Giroud, C., Chazal, N., Gay, B., Eldin, P., Brun, S., Briant, L., 2013. HIV-1-associated PKA acts as a cofactor for genome reverse transcription. Retrovirology 10, 157. https://doi.org/10.1186/1742-4690-10-157.

Gross, I., Hohenberg, H., Wilk, T., Wiegers, K., Grättinger, M., Müller, B., Fuller, S., Kräusslich, H.G., 2000. A conformational switch controlling HIV-1 morphogenesis. EMBO J. 19, 103–113. https://doi.org/10.1093/emboj/19.1.103.

Guo, X., Roldan, A., Hu, J., Wainberg, M.A., Liang, C., 2005. Mutation of the SP1 sequence impairs both multimerization and membrane-binding activities of human immunodeficiency virus type 1 Gag. J. Virol. 79, 1803–1812. https://doi.org/10.1128/JVI.79.3.1803-1812.2005.

Jeener, J., Meier, B.H., Bachmann, P., Ernst, R.R., 1979. Investigation of Exchange Processes by Two-dimensional NMR Spectroscopy. 4546.

Jones, D.T., Miller, R.T., Thornton, J.M., 1995. Successful protein fold recognition by optimal sequence threading validated by rigorous blind testing. Proteins 23, 387–397. https://doi.org/10.1002/prot.340230312.

Jones, G., Willett, P., Glen, R.C., Leach, A.R., Taylor, R., 1997. Development and validation of a genetic algorithm for flexible docking. J. Mol. Biol. 267, 727–748. https://doi.org/10.1006/jmbi.1996.0897.

Kanamoto, T., Kashiwada, Y., Kanbara, K., Gotoh, K., Yoshimori, M., Goto, T., Sano, K., Nakashima, H., 2001. Anti-human immunodeficiency virus activity of YK-FH312 (a betulinic acid derivative), a novel compound blocking viral maturation. Antimicrob. Agents Chemother. 45, 1225–1230. https://doi.org/10.1128/AAC.45.4.1225-1230.2001.

Kashiwada, Y., Hashimoto, F., Cosentino, L.M., Chen, C.H., Garrett, P.E., Lee, K.H., 1996. Betulinic acid and dihydrobetulinic acid derivatives as potent anti-HIV agents. J. Med. Chem. 39, 1016–1017. https://doi.org/10.1021/jm950922q.

Keller, P.W., Adamson, C.S., Heymann, J.B., Freed, E.O., Steven, A.C., 2011. HIV-1 maturation inhibitor bevirimat stabilizes the immature Gag lattice. J. Virol. 85, 1420–1428. https://doi.org/10.1128/JVI.01926-10.

Konvalinka, J., Kräusslich, H.-G., Müller, B., 2015. Retroviral proteases and their roles in virion maturation. Virology 479–480, 403–417. https://doi.org/10.1016/j.virol.2015.03.021.

Kräusslich, H.G., Fäcke, M., Heuser, A.M., Konvalinka, J., Zentgraf, H., 1995. The spacer peptide between human immunodeficiency virus capsid and nucleocapsid proteins is essential for ordered assembly and viral infectivity. J. Virol. 69, 3407–3419.

Li, F., Goila-Gaur, R., Salzwedel, K., Kilgore, N.R., Reddick, M., Matallana, C., Castillo, A., Zoumplis, D., Martin, D.E., Orenstein, J.M., Allaway, G.P., Freed, E.O., Wild, C.T., 2003. PA-457: a potent HIV inhibitor that disrupts core condensation by targeting a late step in Gag processing. Proc. Natl. Acad. Sci. U.S.A. 100, 13555–13560. https://doi.org/10.1073/pnas.2234683100.

Li, G., Verheyen, J., Rhee, S.-Y., Voet, A., Vandamme, A.-M., Theys, K., 2013. Functional conservation of HIV-1 Gag: implications for rational drug design. Retrovirology 10, 126. https://doi.org/10.1186/1742-4690-10-126.

Liang, C., Hu, J., Russell, R.S., Roldan, A., Kleiman, L., Wainberg, M.A., 2002. Characterization of a putative alpha-helix across the capsid-SP1 boundary that is critical for the multimerization of human immunodeficiency virus type 1 gag. J. Virol. 76, 11729–11737.

Liu, Z., Swidorski, J.J., Nowicka-Sans, B., Terry, B., Protack, T., Lin, Z., Samanta, H., Zhang, S., Li, Z., Parker, D.D., Rahematpura, S., Jenkins, S., Beno, B.R., Krystal, M., Meanwell, N.A., Dicker, I.B., Regueiro-Ren, A., 2016. C-3 benzoic acid derivatives of C-3 deoxybetulinic acid and deoxybetulin as HIV-1 maturation inhibitors. Bioorg. Med. Chem. 24, 1757–1770. https://doi.org/10.1016/j.bmc.2016.03.001.

Lu, W., Salzwedel, K., Wang, D., Chakravarty, S., Freed, E.O., Wild, C.T., Li, F., 2011. A single polymorphism in HIV-1 subtype C SP1 is sufficient to confer natural resistance to the maturation inhibitor bevirimat. Antimicrob. Agents Chemother. 55, 3324–3329. https://doi.org/10.1128/AAC.01435-10.

Margot, N.A., Gibbs, C.S., Miller, M.D., 2010. Phenotypic susceptibility to bevirimat in isolates from HIV-1-infected patients without prior exposure to bevirimat. Antimicrob. Agents Chemother. 54, 2345–2353. https://doi.org/10.1128/AAC.01784-09.

Melamed, D., Mark-Danieli, M., Kenan-Eichler, M., Kraus, O., Castiel, A., Laham, N., Pupko, T., Glaser, F., Ben-Tal, N., Bacharach, E., 2004. The conserved carboxy terminus of the capsid domain of human immunodeficiency virus type 1 gag protein is important for virion assembly and release. J. Virol. 78, 9675–9688. https://doi.org/10.1128/JVI.78.18.9675-9688.2004.

Morellet, N., Druillennec, S., Lenoir, C., Bouaziz, S., Roques, B.P., 2005. Helical structure determined by NMR of the HIV-1 (345-392)Gag sequence, surrounding p2: implications for particle assembly and RNA packaging. Protein Sci. 14, 375–386. https://doi.org/10.1110/ps.041087605.

Nowicka-Sans, B., Protack, T., Lin, Z., Li, Z., Zhang, S., Sun, Y., Samanta, H., Terry, B., Liu, Z., Chen, Y., Sin, N., Sit, S.Y., Swidorski, J.J., Chen, J., Venables, B.L., Healy, M., Meanwell, N.A., Cockett, M., Hanumegowda, U., Regueiro-Ren, A., Krystal, M., Dicker, I.B., 2016 Jun 20. Identification and characterization of BMS-955176, a second-generation HIV-1 maturation inhibitor with improved potency, antiviral spectrum, and gag polymorphic coverage. Antimicrob Agents Chemother 60 (7), 3956–3969. https://doi.org/10.1128/AAC.02560-15.

Nguyen, A.T., Feasley, C.L., Jackson, K.W., Nitz, T.J., Salzwedel, K., Air, G.M., Sakalian, M., 2011. The prototype HIV-1 maturation inhibitor, bevirimat, binds to the CA-SP1 cleavage site in immature Gag particles. Retrovirology 8, 101. https://doi.org/10.1186/1742-4690-8-101.

Pettit, S.C., Moody, M.D., Wehbie, R.S., Kaplan, A.H., Nantermet, P.V., Klein, C.A., Swanstrom, R., 1994. The p2 domain of human immunodeficiency virus type 1 Gag regulates sequential proteolytic processing and is required to produce fully infectious virions. J. Virol. 68, 8017–8027.

Qian, K., Bori, I.D., Chen, C.-H., Huang, L., Lee, K.-H., 2012. Anti-AIDS agents 90. novel C-28 modified bevirimat analogues as potent HIV maturation inhibitors. J. Med. Chem. 55, 8128–8136. https://doi.org/10.1021/jm301040s.

Qian, K., Kuo, R.-Y., Chen, C.-H., Huang, L., Morris-Natschke, S.L., Lee, K.-H., 2010. Anti-AIDS agents 81. Design, synthesis, and structure-activity relationship study of betulinic acid and moronic acid derivatives as potent HIV maturation inhibitors. J. Med. Chem. 53, 3133–3141. https://doi.org/10.1021/jm901782m.

Regueiro-Ren, A., Liu, Z., Chen, Y., Sin, N., Sit, S.-Y., Swidorski, J.J., Chen, J., Venables, B.L., Zhu, J., Nowicka-Sans, B., Protack, T., Lin, Z., Terry, B., Samanta, H., Zhang, S., Li, Z., Beno, B.R., Huang, X.S., Rahematpura, S., Parker, D.D., Haskell, R., Jenkins, S., Santone, K.S., Cockett, M.I., Krystal, M., Meanwell, N.A., Hanumegowda, U., Dicker, I.B., 2016. Discovery of BMS-955176, a second generation HIV-1 maturation inhibitor with broad spectrum antiviral activity. ACS Med. Chem. Lett. 7, 568–572. https://doi.org/10.1021/acsmedchemlett.6b00010.

Richards, J., McCallister, S., 2008. Maturation inhibitors as new antiretroviral agents. J. HIV Ther. 13, 79–82.

Schneider, R., Campbell, M., Nasioulas, G., Felber, B.K., Pavlakis, G.N., 1997. Inactivation of the human immunodeficiency virus type 1 inhibitory elements allows Rev-

independent expression of Gag and Gag/protease and particle formation. J. Virol. 71, 4892–4903.
Schur, F.K.M., Obr, M., Hagen, W.J.H., Wan, W., Jakobi, A.J., Kirkpatrick, J.M., Sachse, C., Kräusslich, H.-G., Briggs, J.A.G., 2016. An atomic model of HIV-1 capsid-SP1 reveals structures regulating assembly and maturation. Science 353, 506–508. https://doi.org/10.1126/science.aaf9620.
Seclén, E., González, M. del M., Corral, A., de Mendoza, C., Soriano, V., Poveda, E., 2010. High prevalence of natural polymorphisms in Gag (CA-SP1) associated with reduced response to Bevirimat, an HIV-1 maturation inhibitor. AIDS 24, 467–469. https://doi.org/10.1097/QAD.0b013e328335ce07.
Stoddart, C.A., Joshi, P., Sloan, B., Bare, J.C., Smith, P.C., Allaway, G.P., Wild, C.T., Martin, D.E., 2007. Potent activity of the HIV-1 maturation inhibitor bevirimat in SCID-hu Thy/Liv mice. PLoS One 2, e1251. https://doi.org/10.1371/journal.pone.0001251.
Sundquist, W.I., Kräusslich, H.-G., 2012. HIV-1 assembly, budding, and maturation. Cold Spring Harb. Perspect. Med. 2, a006924. https://doi.org/10.1101/cshperspect.a006924.
Swidorski, J.J., Liu, Z., Sit, S.-Y., Chen, J., Chen, Y., Sin, N., Venables, B.L., Parker, D.D., Nowicka-Sans, B., Terry, B.J., Protack, T., Rahematpura, S., Hanumegowda, U., Jenkins, S., Krystal, M., Dicker, I.B., Meanwell, N.A., Regueiro-Ren, A., 2016. Inhibitors of HIV-1 maturation: development of structure-activity relationship for C-28 amides based on C-3 benzoic acid-modified triterpenoids. Bioorg. Med. Chem. Lett 26, 1925–1930. https://doi.org/10.1016/j.bmcl.2016.03.019.
Tanaka, M., Robinson, B.A., Chutiraka, K., Geary, C.D., Reed, J.C., Lingappa, J.R., 2016. Mutations of conserved residues in the major Homology region arrest assembling HIV-1 gag as a membrane-targeted intermediate containing genomic RNA and cellular proteins. J. Virol. 90, 1944–1963. https://doi.org/10.1128/JVI.02698-15.
Tang, J., Jones, S.A., Jeffery, J.L., Miranda, S.R., Galardi, C.M., Irlbeck, D.M., Brown, K.W., McDanal, C.B., Han, N., Gao, D., Wu, Y., Shen, B., Liu, C., Xi, C., Yang, H., Li, R., Yu, Y., Sun, Y., Jin, Z., Wang, E., Johns, B.A., 2014. Synthesis and biological evaluation of macrocyclized betulin derivatives as a novel class of anti-HIV-1 maturation inhibitors. Open Med. Chem. J. 8, 23–27. https://doi.org/10.2174/1874104501408010023.
Tang, J., Jones, S.A., Jeffrey, J.L., Miranda, S.R., Galardi, C.M., Irlbeck, D.M., Brown, K.W., McDanal, C.B., Johns, B.A., 2017. Discovery of a novel and potent class of anti-HIV-1 maturation inhibitors with improved virology profile against gag polymorphisms. Bioorg. Med. Chem. Lett 27, 2689–2694. https://doi.org/10.1016/j.bmcl.2017.04.042.
Timilsina, U., Ghimire, D., Adhikari, L.P., Bhattarai, A., Mishra, N., Rai, M., Dubey, R.C., Gaur, R., 2018. Maturation inhibitors facilitate virus assembly and release of HIV-1 capsid P224 mutant. Virology 521, 44–50. https://doi.org/10.1016/j.virol.2018.05.024.
Urano, E., Ablan, S.D., Mandt, R., Pauly, G.T., Sigano, D.M., Schneider, J.P., Martin, D.E., Nitz, T.J., Wild, C.T., Freed, E.O., 2015. Alkyl amine bevirimat derivatives are potent and broadly active HIV-1 maturation inhibitors. Antimicrob. Agents Chemother. 60, 190–197. https://doi.org/10.1128/AAC.02121-15.
Urano, E., Timilsina, U., Kaplan, J.A., Ablan, S., Ghimire, D., Pham, P., Kuruppu, N., Mandt, R., Durell, S.R., Nitz, T.J., Martin, D.E., Wild, C.T., Gaur, R., Freed, E.O., 2018. Resistance to second-generation HIV-1 maturation inhibitors. J. Virol. https://doi.org/10.1128/JVI.02017-18.
Van Baelen, K., Salzwedel, K., Rondelez, E., Van Eygen, V., De Vos, S., Verheyen, A., Steegen, K., Verlinden, Y., Allaway, G.P., Stuyver, L.J., 2009. Susceptibility of human immunodeficiency virus type 1 to the maturation inhibitor bevirimat is modulated by baseline polymorphisms in Gag spacer peptide 1. Antimicrob. Agents Chemother. 53, 2185–2188. https://doi.org/10.1128/AAC.01650-08.
von Schwedler, U.K., Stray, K.M., Garrus, J.E., Sundquist, W.I., 2003. Functional surfaces of the human immunodeficiency virus type 1 capsid protein. J. Virol. 77, 5439–5450.
Wagner, J.M., Zadrozny, K.K., Chrustowicz, J., Purdy, M.D., Yeager, M., Ganser-Pornillos, B.K., Pornillos, O., 2016. Crystal structure of an HIV assembly and maturation switch. Elife 5. https://doi.org/10.7554/eLife.17063.
Waheed, A.A., Freed, E.O., 2012. HIV type 1 Gag as a target for antiviral therapy. AIDS Res. Hum. Retrovir. 28, 54–75. https://doi.org/10.1089/AID.2011.0230.
Wainberg, M.A., Albert, J., 2010. Can the further clinical development of bevirimat be justified? AIDS 24, 773–774. https://doi.org/10.1097/QAD.0b013e328331c83b.
Waki, K., Durell, S.R., Soheilian, F., Nagashima, K., Butler, S.L., Freed, E.O., 2012. Structural and functional insights into the HIV-1 maturation inhibitor binding pocket. PLoS Pathog. 8, e1002997. https://doi.org/10.1371/journal.ppat.1002997.
Wang, D., Lu, W., Li, F., 2015. Pharmacological intervention of HIV-1 maturation. Acta Pharm. Sin. B 5, 493–499. https://doi.org/10.1016/j.apsb.2015.05.004.
Wang, M., Quinn, C.M., Perilla, J.R., Zhang, H., Shirra, R., Hou, G., Byeon, I.-J., Suiter, C.L., Ablan, S., Urano, E., Nitz, T.J., Aiken, C., Freed, E.O., Zhang, P., Schulten, K., Gronenborn, A.M., Polenova, T., 2017. Quenching protein dynamics interferes with HIV capsid maturation. Nat. Commun. 8, 1779. https://doi.org/10.1038/s41467-017-01856-y.
Wiegers, K., Rutter, G., Kottler, H., Tessmer, U., Hohenberg, H., Kräusslich, H.G., 1998. Sequential steps in human immunodeficiency virus particle maturation revealed by alterations of individual Gag polyprotein cleavage sites. J. Virol. 72, 2846–2854.
Zhou, J., Chen, C.H., Aiken, C., 2004. The sequence of the CA-SP1 junction accounts for the differential sensitivity of HIV-1 and SIV to the small molecule maturation inhibitor 3-O-{3',3'-dimethylsuccinyl}-betulinic acid. Retrovirology 1, 15. https://doi.org/10.1186/1742-4690-1-15.